Spatial and temporal distribution of fine aerosol acidity in the Eastern Mediterranean

Anna Maria Neroladaki[1,2], Maria Tsagkaraki[1], Kyriaki Papoutsidaki[1], Kalliopi Tavernaraki[1], Filothei Boufidou[3], Pavlos Zarmpas[1], Irini Tsiodra[4], Eleni Liakakou[4], Aikaterini Bougiatioti[4], Giorgos Kouvarakis[1], Nikos Kalivitis[1], Christos Kaltsonoudis[2], Athanasios Karagioras[5], Dimitris Balis[6], Konstantinos Michailidis[6], Konstantinos Kourtidis[5], Stelios Myriokefalitakis[4], Nikos Hatzianastassiou[7], Spyros N. Pandis[2], Athanasios Nenes[2,8], Nikolaos Mihalopoulos[1,3] and Maria Kanakidou[1,2,7]

[1]Environmental Chemical Processes Laboratory (ECPL), Department of Chemistry, University of Crete, 70013 Heraklion, Greece

[2]Center for Studies of Air Quality and Climate Change, Institute for Chemical Engineering Sciences, Foundation for Research and Technology Hellas, 26504 Patras, Greece

[3]Institute of Environmental Physics, University of Bremen, 28359 Bremen, Germany

[4]Institute for Environmental Research and Sustainable Development, National Observatory of Athens, 15236 Palea Penteli, Greece

[5] Department of Environmental Engineering, Democritus University of Thrace, 67100 Xanthi, Greece

[6]Laboratory of Atmospheric Physics, Aristotle University of Thessaloniki, 54634 Thessaloniki, Greece

[7]Laboratory of Meteorology, Department of Physics, University of Ioannina, 45110 Ioannina, Greece

[8]Laboratory of Atmospheric Processes and their Impacts, School of Architecture, Civil and Environmental Engineering, Ecole Polytechnique Fédérale de Lausanne, 1015, Lausanne, Switzerland

Correspondence to: Maria Kanakidou (mariak@uoc.gr)

Abstract. Aerosol acidity (pH) affects aerosol composition and properties, and therefore climate, human health and ecosystems. Fine aerosol acidity and its seasonal variation at 6 sites (Finokalia, Patras, Thissio, Ioannina, Thessaloniki, and Xanthi) in Greece were investigated during 2019-2020. The thermodynamic model ISORROPIA-lite was used to calculate aerosol water and acidity based on measurements of the chemical composition of $PM_{2.5}$ and available gas-phase concentrations of HNO_3, NH_3, and HCl. During winter the fine aerosols were acidic to moderately acidic throughout Greece with an overall mean aerosol pH of 3.57 ± 0.44 in urban areas and 3.05 ± 0.50 in remote locations. The highest aerosol pH (4.08 ± 0.42) in January 2020 was found in Ioannina due to, among others, high K^+ levels from biomass burning emissions. Aerosols in Xanthi were the most acidic due to high sulfate levels. Similar seasonal profiles of aerosol pH were observed at all sites studied with different factors contributing to this seasonality. During the summer $PM_{2.5}$ at Thissio, Ioannina and Finokalia was acidic with a mean aerosol pH across all three sites of 1.76 ± 0.40. During this season, sulfates were the driver of the higher acidity conditions at Thissio and Finokalia, with other factors such as the semivolatiles and temperature contributing to a lesser extent. At Ioannina, temperature along with the total ammonia and nitrate were the main contributors to the seasonal difference of the aerosol pH, while some of the nonvolatile species also contributed. In most cases, the importance of organics for aerosol pH was small.

1 Introduction

42 The aerosol pH is one of the most important chemical properties of aerosols. It controls the rates of several
43 reactions in the particulate phase (e.g., sulfate and oligomer formation reactions in the particulate phase) and
44 governs the gas-particle partitioning of semivolatile gases such as ammonia (NH_3), nitric acid (HNO_3) and
45 hydrochloric acid (HCl), and some organic acids with low molecular weight (formic, oxalic, acetic etc.) and bases
46 (e.g. amines). Several studies have thoroughly discussed the importance of the gas phase NH_3 and HNO_3 and their
47 effect on the particulate matter as well as their relationship with aerosol pH and water (Pye et al., 2020; Nenes et
48 al., 2020; Guo et al., 2018, 2016, 2017b). NH_3 from anthropogenic and biogenic emissions is the most important
49 gaseous base in the atmosphere, while HNO_3 is an acid produced by the oxidation of NO_x mainly emitted by
50 combustion sources (Seinfeld and Pandis, 2006). HNO_3, because of its strong acidity and solubility, partitions
51 more in the gas phase than in the particle phase (as nitrate) at lower aerosol pH (usually below 1.5 to 2) (Weber
52 et al., 2016), while NH_3 remains in the gas phase at higher pH. These processes have serious implications for the
53 wet and dry deposition of these semivolatile pollutants on ecosystems, their lifetime, climate and human health
54 (Pye et al., 2020).

55 Metal cations, including those that originate from dust and sea salt, are nonvolatile at atmospheric
56 temperatures. These constituents seriously affect the aerosol pH together with parameters such as the
57 meteorological conditions (i.e. temperature and relative humidity). These parameters and the availability of
58 sulfuric acid (that partitions almost exclusively to the particulate phase) are mostly responsible for the wide range
59 of the pH of atmospheric particles (Pye et al., 2020).

60 Aerosol pH affects the uptake of sulfur dioxide (SO_2) into the aerosol aqueous phase and its oxidation to sulfate
61 (Seinfeld and Pandis, 2006). This is important for climate, as sulfate is one of the main scattering components of
62 atmospheric aerosols with a cooling effect on climate. Acid catalyzed reactions lead to the formation of brown
63 carbon that is an important contributor to absorbing aerosol (Zhang et al., 2020). Atmospheric acidity affects
64 aerosol toxicity, controlling the solubilization of toxic forms of transition and heavy metals, such as copper and
65 iron (Fang et al., 2017) with adverse impacts on human health (Vierke et al., 2013). Furthermore, acidity increases
66 the solubility and thus the bioavailability of iron, phosphorus and trace metals that are deposited on ecosystems
67 (Pye et al., 2020). This is of a great importance in oligotrophic areas, such as the East Mediterranean Sea, a marine
68 desert, characterized by extremely low biological productivity, due to the limited availability of nutrients like
69 phosphate (Powley et al., 2017). The area is frequently influenced by dust outbreaks from the Saharan desert,
70 which contain several minerals and metals primarily in insoluble forms. The conversion of insoluble to soluble
71 bioavailable form of a given nutrient is favored under acidic conditions (Kanakidou et al., 2018; Nenes et al.,
72 2011). The solubility of iron and thus its bioavailability to ecosystems, is also controlled by acidity, as it is
73 enhanced in the presence of acidic species. Theodosi et al. (2008) found that in the Eastern Mediterranean the iron
74 solubility ranged from 28% for polluted rainwater (pH 4-5) to 0.5% for Sahara dust episodes (pH=8).

75 Although the acidity of atmospheric particles plays such a critical role in all of the atmospheric processes
76 mentioned above, there is no direct method for its accurate measurement due to the miniscule sample mass and
77 liquid volume (Pye et al., 2020). Thus, several indirect methods have been developed, which estimate aerosol
78 acidity (Pye et al., 2020). One of the best available methods is the aerosol pH prediction using atmospheric aerosol
79 thermodynamic models in combination with measurements of aerosol composition and gas-phase HNO_3, NH_3 and
80 HCl concentrations. Models such as ISORROPIA II (Fountoukis and Nenes, 2007), MOSAIC (Zaveri et al.,
81 2008), E-AIM; (Clegg et al., 2001; Wexler and Clegg, 2002), etc. can be used to this purpose.

82   Aerosols' acidity covers a wide range and aerosol pH can be as high as about 7 pH units (sea salt), and as low

83   as -1 and sometimes even -2 pH units, depending on the composition of the aerosol and the meteorological

84   conditions in a given area (Pye et al., 2020). Negative values appear when sulfates are the dominant constituent

85   of particulate matter, while the aerosol pH rarely rises above neutral levels (pH = 7). Globally fine atmospheric

86   particles ($PM_{2.5}$) have been found to have a bimodal acidity pattern with one population of smaller particles having

87   an average pH between 1 and 3 pH units, and another of larger particles with a mean pH close to 4 and 5 units,

88   which is due to the influence of dust, sea spray and biomass burning (Sindosi et al., 2012; Pye et al., 2020).

89   Several studies have investigated the levels of the acidity of fine particles and their major drivers at specific

90   sites. For instance, studies in Beijing and close-by locations indicate a mean wintertime $PM_{2.5}$ pH of 4.2 to 4.9

91   units (Liu et al., 2017; Guo et al., 2017a; Shi et al., 2017; Ding et al., 2019). Pye et al. (2020) summarized and

92   investigated the fine aerosol pH in several regions globally and reported that overall aerosol pH is consistently

93   acidic and looking into the seasonality, during wintertime where low temperature and high relative humidity

94   occur, aerosol pH was higher compared to summertime following the temperature and the availability of liquid

95   water content. Tao and Murphy (2019) reported that in winter the pH of fine aerosols was around 3 units at 6 sites

96   in Canada and was strongly influenced by temperature, relative humidity and aerosol chemical composition.

97   Kakavas et al. (2021) simulated the aerosol acidity and its variation with size and altitude over Europe during

98   summer and found the ground level mean aerosol pH across the domain to be 2.05 for PM_1, 2.65 for $PM_{1-2.5}$, 3.2

99   for $PM_{2.5-5}$ and 3.35 for PM_{5-10}. The lowest aerosol pH was reported in the Mediterranean and especially in the

100   eastern Mediterranean where high sulfate and nitrate levels were predicted. This study suggests that Eastern

101   Mediterranean can be an especially interesting region for aerosol pH studies.

102   There have been only limited estimations of aerosol acidity in the eastern Mediterranean. The $PM_{2.5}$ pH in 6

103   cities in the eastern Po Valley in Italy (Masiol et al., 2020) was found to range from 1.5 to 4.5 with summer

104   minima and winter maxima and mean pH values across all sites of 2.2 ± 0.3 and 3.9 ± 0.3, respectively. These

105   levels of fine aerosol acidity were mainly driven by secondary sulfate, fossil fuel combustion, secondary nitrate

106   and biomass burning. An earlier study in the same area (Squizzato et al., 2013) investigated seasonally the aerosol

107   pH and found that in spring the aerosol pH was higher compared to summer (average aerosol pH across the sites;

108   spring 3.6 pH units, summer 2.3, autumn 3, winter 3.6) as a result of desert dust aerosol originating from the

109   Sahara desert. Again in Po Valley, a multiyear (25 years) trend of fog water pH and aerosol pH was estimated

110   (Paglione et al., 2021) and an opposite trend between them was found; there was an increase in the fog water pH

111   and a decrease in fine aerosol acidity. In fact, there was a decrease of 0.5-1.5 pH units in the aerosol pH that was

112   driven by the contemporary decrease of the corresponding air pollutants due to environmental policies in

113   combination with the changing meteorology (temperature and relative humidity levels). Lastly, the submicron

114   aerosol pH was estimated in a study conducted at the Finokalia atmospheric observation station in Greece

115   (Bougiatioti et al., 2016) and was found to be highly acidic ranging from 0.5 to 2.8 pH units with daytime

116   minimum and nighttime maximum values due to low aerosol water content and high temperatures during the day.

117   They also pointed out the influence of biomass burning which increased the aerosol pH values highlighting the

118   impact of nonvolatile cations, mainly potassium from biomass burning together with ammonia and nitrate emitted

119   from wood burning. Despite these studies, the spatial distribution of aerosol acidity based on atmospheric

120   composition observations is not well understood.

121 The present study aims to provide a spatial and seasonal picture of the acidity of fine ($PM_{2.5}$) atmospheric
122 aerosol over Greece in the eastern Mediterranean based on observations of atmospheric composition. For this, the
123 ISORROPIA-lite thermodynamic equilibrium model (Kakavas et al., 2022) is used together with observations of
124 the chemical composition of the fine aerosol from 6 sites over Greece and with gas phase NH_3 and HNO_3 data,
125 where available. The water and pH of the fine aerosol are estimated during summer 2019 and winter 2019-2020.
126 The factors controlling the seasonality of aerosol pH are examined and the effect of particulate organic matter on
127 aerosol pH predictions is also investigated.

128 **2 Measurements and Methodology**

129 2.1 Measurement sites

130 Measurements of the chemical composition of $PM_{2.5}$ were performed at 6 sites across Greece (Fig. 1) (Finokalia,
131 Thissio, Patra, Ioannina, Xanthi and Thessaloniki, Table S1). The corresponding summer and winter field
132 campaigns were conducted within the PANACEA (PANhellenic infrastructure for Atmospheric Composition and
133 climatE chAnge) project during the summer of 2019 (at 3 of the sites, Finokalia, Thissio and Ioannina) and the
134 winter of 2019-2020 (at all sites).

135 The Finokalia atmospheric observatory of the University of Crete in Crete, Greece (FKL, 35.33º N, 25.67º E;
136 250 m a.s.l) is a remote regional background site in the northeast coast of the island of Crete (south Greece). The
137 site is not subject to any major anthropogenic influence and it is considered as a representative background site
138 for the entire eastern Mediterranean. During the warm months of the year (April to September, dry season) the
139 station mainly receives air masses from the N/NW (originating from the Central and Eastern Europe and the
140 Balkans), while between October and April (wet season) air masses coming from the South lead to Saharan dust
141 events (Mihalopoulos et al., 1997).

142 The Thissio Air Monitoring station (THI, 37.97º N, 23.72º E, 105 m a.s.l.) of the National Observatory of
143 Athens, Greece is located approximately 50 m above the mean city level near the historical city center. The station
144 is an urban background site due to its distance from traffic and industrial emission sources and receives air
145 pollutants from various urban and regional sources.

146 The Patras site is located at the Institute of Chemical Engineering Sciences (ICE-HT) of FORTH (Foundation
147 for Research and Technology, Hellas), which is in Platani (PTR, 38.30º N, 21.81º E, 100 m a.s.l.) 8 km from the
148 city center. It is an urban background site. Local sources include transportation, biomass burning (both residential
149 and agricultural) and shipping emissions, while long-range transport is the dominant $PM_{2.5}$ source during most
150 periods (Pikridas et al., 2013).

151 The Xanthi station is operated by the Laboratory of Atmospheric Pollution and Pollution Control Engineering
152 of Atmospheric Pollutants of the Department of Environmental Engineering. The station is located in the
153 Kimmeria DUTH campus (XAN, 41.15º N, 24.92º E; 75 m a.s.l.) almost 2 km from the city of Xanthi in
154 northeastern Greece. The station is a rural site and the edge of a slope facing to the south, 20 km away from the
155 seashore. The Rodopi Mountain Range is located to the north of the station. The prevailing winds that reach the
156 site in winter are fairly stable SW/S/SE during the day, but they change to N/NW at night; the location of the site

between mountains and a valley creates a closed circulation cell of valley/land breezes (Kastelis and Kourtidis, 2016).

The Thessaloniki station at the north of Greece is at the Laboratory of Atmospheric Physics (LAP) which is located at the School of Sciences of the Aristotle University of Thessaloniki (LAP, 40.63°N, 22.95°E; 50m a.s.l.). Thessaloniki is a coastal city at Thermaikos Gulf and is the second largest city in Greece. The site experiences air pollution episodes due to the meteorological conditions over northern Greece; with high pressure, anticyclonic systems and sunny weather in summer, while colder temperatures near the surface and snow occur in winter (Flocas et al., 2009). It is considered as a representative urban station.

Ioannina (IOA, 39.653195°N, 20.854208°E) is located in Epirus Region in northwestern Greece, which is separated from the eastern part of the country mainland by the Pindus mountain range (orientated from NW to SE and exceeding 2000 m in height). The sampling station was located at a kindergarten yard, 1.5 km from Ioannina's city center. Ioannina is located on a plateau of about 500 m altitude and is surrounded by mountains. The city is next to the Pamvotis lake and is characterized by frequent fog events in winter, due to increased relative humidity, weak winds and basin-like attributes and winter biomass burning events (Kaskaoutis et al., 2020).

2.2 Measurements

The PANACEA campaigns took place at the 6 sites discussed above during the summer of 2019 (at FKL, THI, IOA) and the winter of 2019-2020 (at all 6 sites). Atmospheric particles were collected daily on quartz-fiber filters using high-volume or low-volume aerosol samplers depending on the site. A Sunset Organic Carbon (OC) /Elemental Carbon (EC) analyzer was used to determine the concentrations of OC and EC, while the inorganic cations: ammonium (NH_4^+), potassium (K^+), calcium (Ca^{2+}), magnesium (Mg^{2+}), sodium (Na^+) and anions: sulfate (SO_4^{2-}), chloride (Cl^-), nitrate (NO_3^-) were determined using ion chromatography. Details on the methods of the $PM_{2.5}$ filter analysis during the PANACEA winter and summer campaign can be found in (Kaskaoutis et al., 2022). In situ-measurements of temperature and relative humidity were also available for the period of the campaigns (Fig S1 and S2).

For the campaign period there were not available gas phase concentrations (NH_3, HNO_3) measurements at any of the 6 sampling sites except PTR (NH_3). Thus, for NH_3, satellite data were used for the remaining sites (except IOA during the winter campaign period). For HNO_3, past in situ measurements were used at FKL and for the other sites (THI, PTR, IOA, LAP, XAN) past in situ measurements conducted at THI were used. A summary of the type of NH_3 and HNO_3 measurement data used (satellite or in-situ, simultaneous or past, same or neighbor site), is presented in Table S2 of the supplement.

In more detail, the Patras site as mentioned above, was the only site with available gas-phase NH_3 measurements for the studied periods during the 2019-2020 winter campaign, with mean NH_3 concentration of 2.54 ± 0.90 μg/m³. At IOA during the wintertime period of the study, neither in situ observations nor satellite data were available and thus NH_3 observations at PTR were used for IOA. Therefore, the mean NH_3 concentration value from PTR dataset was also used for the IOA wintertime simulations.

For the other sites (FKL and THI during winter and summer, and LAP and XAN during winter) NH_3 data (level 2 data, version 1.6.3) were used from the Cross-track Infrared Sounder (CrIS) instrument which is deployed on board the Suomi National Polar-orbiting Partnership (SNPP) platform (into an orbit with an altitude of 824 km

195 above the Earth surface) (Shephard and Cady-Pereira, 2015). NH_3 values over these sites were obtained from the

196 CrIS Fast Physical Retrieval (CFPR) product, which provides NH_3 concentration data for a total of 15 vertical

197 levels, with the value closest to the ground being taken as the near-surface concentration. From the available CrIS

198 near-surface NH_3 concentrations within a 50-km diameter area around each site, the value within the pixel at the

199 closest distance to the site is retained (Shephard et al., 2020; Shephard and Cady-Pereira, 2015). The wintertime

200 near-surface NH_3 concentrations as derived from CrIS for FKL, THI, XAN and LAP are shown in Fig. 2. For

201 summer at FKL and THI, mean values of summertime near-surface NH_3 (from 13/08/2019 to 19/08/2019 for FKL

202 and from 13/08/2019 to 31/08/2019 for THI) are 1.24 ± 0.61 $\mu g/m^3$ and 1.32 ± 1.53 $\mu g/m^3$ respectively, were used

203 due to the scarcity of summertime data from CrIS in 2019.

204 For IOA during summer, a mean NH_3 concentration of 1.04 $\mu g/m^3$ was used as derived from the Atmospheric

205 Infrared Sounder (AIRS) aboard NASA's Aqua satellite (Level 3 data) operating from September 2002 to August

206 2016 (Warner et al., 2016) (the mean summertime 2002-2016 concentration was used).

207 For HNO_3 and HCl gas-phase concentration measurements, samples were collected only at Finokalia (2015 -

208 2016) using glass fiber filters coated with Na_2CO_3 and were analyzed by ion chromatography. The median of

209 these gas-phase measurements of HNO_3 and HCl were used here (0.63 $\mu g/m^3$ and 0.98 $\mu g/m^3$ for winter and 0.95

210 $\mu g/m^3$ and 1.34 $\mu g/m^3$ for summer, respectively). For all other sites, gas-phase measurements of HNO_3 conducted

211 at Thissio from 12/2014 to 3/2016 (Liakakou et al., 2022) were used here as mean values (0.53 ± 0.12 $\mu g/m^3$ for

212 winter and 0.91 ± 0.29 $\mu g/m^3$ for summer).

213 Since the NH_3 in situ observations at PTR did not coincide with any CrIS or AIRS data, a comparison between

214 in situ and satellite data was not possible. The sensitivity of our pH estimates to these assumed NH_3 and HNO_3

215 concentrations will be examined in a subsequent section (see section 3.4).

216

217 2.3 pH Estimation

218 The pH of the fine aerosol at the 6 studied sites, was calculated using ISORROPIA-lite thermodynamic model

219 (Kakavas et al., 2022), which is an extension of the ISORROPIA-II model (Fountoukis and Nenes, 2007).

220 ISORROPIA-lite treats the same system of aerosols as ISORROPIA-II (Ca^{2+}, K^+, Mg^{2+}, SO_4^{2-}, Na^+, NH_4^+, NO_3^-,

221 Cl^-, H_2O and their equilibrium with the gas phase HNO_3, NH_3, HCl and H_2O) with the addition of the organic

222 aerosol and considering only the deliquescent aerosol at all RH values. The addition of organic matter in the

223 thermodynamic equilibrium aerosol system, results in more aerosol water which favors the partitioning of

224 semivolatile inorganic species into the aerosol phase in order to satisfy the equilibrium (Kakavas et al., 2022).

225 The particle water (W_{org}) associated with the organic aerosol is implemented in the model using the hygroscopicity

226 parameter (κ_{org}). The total aerosol water content, i.e. the water associated with the inorganic and organic parts of

227 the aerosol, is the sum of the inorganic and organic water and it is used in the thermodynamic calculations. The

228 aerosol pH is then calculated by:

230
$$pH = -\log_{10} \frac{1000 \, \gamma_{H^+} \, [H_{air}^+]}{[W_{inorg}] + [W_{org}]}$$

229 (1)

231 where γ_{H+} is the activity coefficient of the hydronium ion (H$^+$) here assumed unity, H$^+_{air}$ is the equilibrium particle

232 hydronium ion concentration per volume air (μg/m^3), W$_{inorg}$ and W$_{org}$ is the water associated with the inorganic

233 and organic part of the aerosol, respectively (both in μg/m^3). Thus, the aerosol pH was calculated including the

234 contribution of the organic aerosol hence the aerosol water associated with both inorganic and organic species.

235 Daily values were used as input to the model. These were gas phase (NH$_3$, HNO$_3$) and particulate phase (ions and

236 OA) concentrations, OA hygroscopicity and density, and meteorological data (temperature and relative humidity).

237 To calculate the aerosol water content associated with the organic species, the total organic aerosol

238 concentration (OA) derived from the OC measurements at each site is used together with an OA/OC ratio of 1.8

239 for all sites. This average ratio is consistent with the results of measurements conducted at the same sites (Florou

240 et al., 2017; Hildebrandt et al., 2011; Kaskaoutis et al., 2020, 2022; Kostenidou et al., 2015; Pikridas et al., 2013;

241 Stavroulas et al., 2019; Tsiflikiotou et al., 2019). The hygroscopicity parameter was set to κ_{org}= 0.16 for Finokalia

242 as suggested in studies for this site (Bougiatioti et al., 2009; Kalkavouras et al., 2019), and κ_{org}=0.12 for the other

243 sites (Psichoudaki et al., 2018).

244 **3 Results and Discussion**

245 3.1 Aerosol Composition

246 The chemical composition and mass concentration of the major species in PM$_{2.5}$ measured during the PANACEA

247 campaigns are summarized in Table 1. The dominant PM$_{2.5}$ component was OA at all sites except FKL, where

248 sulfate dominated both in winter and summer. This is typical for remote background sites (Lemou et al., 2020;

249 Sciare et al., 2008). Higher sulfate levels were present in FKL during summer due to high temperatures and

250 photochemistry, followed by organics (typically consisting 20-30% of the PM$_{2.5}$ mass, Pikridas et al., 2010; Putaud

251 et al., 2004). The highest levels of OA were observed at Ioannina (IOA) during winter. OA represented more than

252 60% of the PM$_{2.5}$ and was mainly due to residential wood burning emissions while the meteorology and

253 topography of the area facilitated the accumulation of all pollutants (Kaskaoutis et al., 2022). Much lower levels

254 of OA and PM$_{2.5}$ mainly of regional origin, were measured at IOA in the summer (Kaskaoutis et al., 2022). At the

255 three sites where measurements were available in the summer (IOA, FKL, THI), sulfate was a major component

256 of the PM$_{2.5}$ despite their different characteristics. Inorganic PM$_{2.5}$ across all sites in winter was dominated by

257 sulfate except IOA where, interestingly, NO$_3^-$ was the dominant inorganic PM$_{2.5}$ component due to possible high

258 NO$_x$ emissions, or NO$_x$ accumulation in the boundary layer due to low inversion heights and decreased horizontal

259 circulation, the latter due to surrounding mountains. The K$^+$ levels in IOA were also elevated indicating the

260 influence of biomass burning in the area (Kaskaoutis et al., 2022).

261

262 3.2 Aerosol pH across Greece

263 3.2.1 Winter

264 The distributions of estimated pH of PM$_{2.5}$ as derived from the ISORROPIA-lite model for the 6 studied sites

265 during winter (January 2020) is shown in Fig. 3a. Due to the lack of data in some of the sites during the winter

2019-2020, the results of only January 2020 were used in order to be able to compare the aerosol pH results among the sites. The entirety of the aerosol pH results for all sites during winter 2019-2020 can be found in Fig. S4.

In January the aerosols at THI were slightly acidic with a wide range of pH values (2.17 to 4.17), reflecting the variation of the $PM_{2.5}$ composition and meteorology. The mean pH was 3.30 ± 0.48 (median 3.34). Days with highly acidic aerosol, i.e. pH below 2.5, were associated with elevated sulfate levels and northerly winds. At FKL the mean aerosol pH was 3.25 ± 0.37 and ranged from 2.73 to 3.89 (median 3.30). The elevated pH coincided with high concentrations of nonvolatile cations (NVC) and NH_3 and the lower pH values (less than 2.8) occurred during periods with high levels of sulfates. In the northern part of Greece, at XAN the pH range covered 2.24 units with a mean value of 2.81 ± 0.53 (median 2.69). The shift between acidic and moderately acidic conditions was associated with changes mainly in NH_3 and sulfate levels. Days when pH reached almost 4, were characterized by high K^+ in combination with high OA and EC levels and low sulfates suggesting significant influence of biomass burning. At LAP the pH of $PM_{2.5}$ ranged from 2.72 to 3.41, with a mean value of 3.01 ± 0.31. Please note that only 4 days of $PM_{2.5}$ measurements were available in LAP during January 2020. The fine aerosol in IOA had the lowest overall acidity with a mean value of 4.08 ± 0.42 units and a range between 3.55 and 5.14 units. These levels of acidity are a consequence of the intense biomass burning during this winter campaign at IOA (Kaskaoutis et al., 2022). Elevated K^+ levels were observed, due almost entirely to wood burning for heating. Comparing IOA with the other sites in January, there is a statistically significant difference in aerosol acidity levels due to higher Ca^{2+}, K^+ and NH_3 combined with lower temperature, despite the high sulfates levels in the area (Table 1). At PTR aerosol pH ranged from 2.82 to 4.44 units with a mean value of 3.70 ± 0.45. NVCs (Ca^{2+}, K^+, Mg^{2+} and Na^+), NH_3 and sulfates drove the variability of the aerosol pH most of the days. Aerosols at LAP and XAN exhibited the highest acidity (lowest pH levels) among all studied sites, while IOA and PTR exhibited the highest aerosol pH levels (Fig. 3a). Remarkably, aerosol acidity at the urban background site (THI) was similar to that at the coastal background site (FKL). On the other hand, the suburban site (PTR) had higher aerosol pH mainly due to the likely higher NH_3 levels at PTR than THI and FKL (Table 1), considering though the different ways NH_3 was measured for these sites. Considering the two remote rural and coastal areas (XAN and FKL), their fine aerosol pH differed by about half a pH unit due to increased Na^+, Mg^{2+} and relative humidity levels at FKL together with slightly higher sulfate concentrations at XAN.

The accuracy of the aerosol pH predictions using ISORROPIA-lite was evaluated by comparing the observed with the predicted partitioning coefficient of NH_4^+ ($\varepsilon(NH_4^+)$) and this comparison was possible only at PTR during winter when both NH_3 and NH_4^+ were measured. A useful way to assess the reliability and potential uncertainties of such models' predictions of aerosol pH is the comparison between measured and simulated gas-particle partitioning fractions of semivolatile species (Guo et al., 2016). Figure 4 shows the comparison of the observed and predicted $\varepsilon(NH_4^+)$ calculated for the case of PTR in winter. We focus on PTR since it was the only site where NH_3 in-situ measurements were available making it a more suitable case for such comparison. The measurements and predictions of total NH_3 are well correlated ($R^2=0.78$) although the model underestimates by 30% the $\varepsilon(NH_4^+)$. A sensitivity test and a re-evaluation of the model discussed in the supplementary section S4 (Fig S3) indicates that this small underestimation can be attributed to the uncertainty in the HNO_3 levels. Sensitivity tests regarding the gas phase NH_3 and HNO_3 used to estimate aerosol pH are also provided (section 3.4). Overall, $PM_{2.5}$ during winter varied acidic to moderately acidic with an average pH across all studied urban and urban background sites of 3.57 ± 0.44. The overall $PM_{2.5}$ pH range across all 6 sites was from 1.72 to 5.14.

3.2.2 Summer

The seasonal variation of the acidity of $PM_{2.5}$ was investigated at three of the sites, THI, FKL and IOA in which measurements were available for the summer 2019 PANACEA campaign. The mean $PM_{2.5}$ composition is summarized in Table 1. During the whole period, $PM_{2.5}$ at the three sites was acidic with a mean pH of 1.35 ± 0.18 at THI, 1.75 ± 0.62 at IOA and 2.08 ± 0.45 pH at FKL (Figure 3c). At THI the $PM_{2.5}$ pH was consistently low throughout the summer period with a minimum value of 1.13, and a maximum of 2. At IOA and FKL the $PM_{2.5}$ pH was slightly higher than at THI. At FKL relative humidity levels increased the aerosol water content and together with the relatively high K^+ and Na^+ levels led to higher aerosol pH. Higher Ca^{2+} and K^+ levels at IOA and slightly higher sulfate levels at THI seemed to be the factors controlling the difference in the aerosol pH between these two sites. Overall, comparing the summertime (July and August) aerosol pH levels at the three sites (Fig. 3c and S5), a uniformity can be observed with high aerosol acidity being the case on most of the days, dropping even below 0 at IOA as a result of increased temperature and sulfate levels and reduced aerosol water. FKL and IOA had similar aerosol pH levels since most of the major aerosol components had similar concentrations at the two sites. The higher Ca^{2+}at IOA was balanced by the higher Na^+ in FKL.

3.2.3 Impact of organics

In order to investigate the potential effect of OA on the aerosol pH levels, ISORROPIA-lite was also run considering only the inorganic components of the aerosol (i.e. setting the OA concentration to zero). The mean difference between the aerosol pH calculated considering all aerosol components, including organics and the one accounting only for the inorganic content of $PM_{2.5}$ is shown in Figs. 3b and d for January 2020 and summer 2019, respectively. The water associated with the OA in most cases reduces the H^+ concentration and therefore increases the aerosol pH (Kakavas et al., 2022). However, this expected increase in aerosol pH due to OA was not always found at all sites, because of the resulting changes in the partitioning of the semivolatile compounds from the gas phase to the aerosol phase. This partitioning affects the OA induced change in the H^+ concentration (H^+_{air} concentration in eq. 1), which together with aerosol water determine the aerosol pH.

In January at IOA, THI and PTR, the addition of aerosol water associated with the OA did not always increase the overall aerosol pH. In fact, a mean decrease of about 0.3 pH units was found at IOA, which had the highest OA concentrations among the 3 sites. Figure 5a depicts the aerosol water associated only with the inorganics along with the total one (i.e. including the OA water) and relative humidity and in Fig 5b the timeseries of the aerosol pH at IOA is shown in which again the one associated only with the inorganics and the one including the OA water (total aerosol pH) is depicted. An increase in the aerosol pH as a result of the addition of the organics is clear only at the end of January (from 26-01 to 29-01); the total aerosol pH was higher than the one when OA was absent (by 0.19 pH units on average). This was due to the high aerosol water content, which resulted from high relative humidity (above 80%). The addition of the OA increased aerosol water even more (Fig 5a). On all the other days in January with lower relative humidity, the addition of OA resulted in relative small increases in aerosol water. The partitioning of the semivolatile species to the aerosol phase increased, by decreasing the gas phase concentration (change up to 0.10 μg/m³ for NH_3, 0.18 for HNO_3 and 0.12 for HCL), and similarly increasing the corresponding aerosol phase (NH_4^+, NO_3^- and Cl^-). Furthermore, addition of considerable amounts of aerosol

water affects the activity coefficients of all ionic species (especially sulfate/bisulfate ions and NH_4^+), which shifts the ionic balance slightly. In addition, the free H^+ approximation of pH that we are using (eq.1) does not consider shifts in the activity coefficient in H^+ (Pye et al., 2020). Overall, the increase in the concentrations of the acids exceeded that of ammonium, therefore the concentration of H^+ increased. The increase in aerosol water did not counterbalance the increase in H^+ concentration resulting in a more acidic aerosol (lower aerosol pH). The highest decreases in pH were observed in days where high aerosol pH occurred (inorganic aerosol pH above 4.5 units, mean pH decrease 0.58 units). At the other two sites the aerosol pH decreased by about 0.08 pH units at THI and 0.01 at PTR. These relatively rare, but still important, set of conditions require further tests of thermodynamic model pH predictions.

At FKL, XAN and LAP a small increase in aerosol pH was found; 0.001, 0.05, 0.05 pH units increase respectively. In the summer (July and August), the pH increased at all sites when considering OA water, with the highest predicted increase of about 0.15 at IOA. At the other sites the aerosol pH increased by about 0.09 units at FKL and 0.11 at THI. Therefore, the effect of the organics on the pH at all sites was on average less than 0.3 units.

3.2.4 Main factors controlling seasonality of pH

A clear seasonal difference in acidity was observed at all sites. In summer $PM_{2.5}$ at FKL was 1 pH unit more acidic than in winter. To determine the main drivers of aerosol pH seasonal variability, a series of sensitivity simulations were performed using the concentrations of aerosol components and meteorological conditions observed in winter and replacing each time one of them by its corresponding mean value in summer. Then, the difference in the estimated aerosol pH was calculated. The factors that were tested were: temperature, relative humidity, TNO_3 (sum of gas-phase HNO_3 and particulate NO_3^-), TNH_3 (sum of gas-phase NH_3 and particulate NH_4^+), sulfates, Na^+, K^+, Ca^{2+} and OA. The results for FKL are shown in Fig. 6f and Table S5 as ΔpH, that is the pH of the base case simulation minus that of the perturbation scenario. Sulfate was the main contributor to the change in aerosol acidity between summer and winter at FKL, where the 2 $\mu g\ m^{-3}$ concentration difference between the two seasons resulted in 1.66 units of pH difference. Total NH_3 availability was the second most important factor with a mean ΔpH of 0.39 followed by temperature (mean $\Delta pH = 0.30$) and Na^+ (mean $\Delta pH = 0.25$). The effect of the remaining factors was on average less than 0.20 pH units; TNO_3 (mean $\Delta pH = 0.17$), relative humidity (mean $\Delta pH = 0.16$), K^+ (mean $\Delta pH = 0.15$), Ca^{2+} (mean $\Delta pH = 0.14$) and OA (mean $\Delta pH = 0.08$).

At IOA, aerosol average pH levels differed by 2.26 pH units between summer and winter with higher aerosol pH in winter (Fig. 6a). Simulations were performed using ISORROPIA-lite for nine factors: temperature, relative humidity, TNO_3 (sum of gas-phase HNO_3 and particulate NO_3^-), TNH_3, SO_4^{2-}, Na^+, K^+, Ca^{2+} and OA. The results are shown in Fig. 6b and Table S6. The availability of total HNO_3 ($\Delta pH=0.98$), temperature ($\Delta pH=0.76$) and the total NH_3 ($\Delta pH=0.59$) had the greatest influence on the seasonal aerosol pH difference. The effect of K^+ ($\Delta pH=0.53$), sulfates ($\Delta pH=0.45$) and Ca^{2+} ($\Delta pH=0.43$), followed by organics (0.22), RH (0.21) and Na^+ (0.06) were also notable. High concentrations of K+ affecting the aerosol pH are associated with biomass burning as discussed in Kaskaoutis et al., (2022).

THI also exhibited a significant seasonal difference in the aerosol acidity with $PM_{2.5}$ being approximately 2.6 times more acidic in summer than in winter (Fig. 6c). Nine sensitivity tests were conducted for the effect of the nine factors tested for the other two sites on pH (Table S7, Fig. 6d). Sulfate was found to be the main contributor

to the more acidic conditions in summer at THI with a mean absolute difference in pH (winter - summer), ΔpH, of 2.8 units, followed by TNH$_3$ and temperature with absolute ΔpH of 0.48 and 0.42 units, respectively. The other factors contributed less to the seasonal difference in aerosol pH, with an absolute ΔpH varying between 0.10 and 0.33 units.

3.3 Aerosol water

ISORROPIA-lite can also be used to calculate the contribution of each inorganic salt and organic fraction to the total aerosol water content. Fig. 7 depicts the average contributions of the various inorganic salts and of OA to the total aerosol water for all sites in winter (January) (Fig. 7a) and summer (July and August) (Fig. 7b).

In January (Fig. 7a), OA contributed 60% to the total aerosol water at IOA and 55% at PTR. These were the two sites with the highest levels of OA mainly due to residential wood burning. At LAP and THI, OA was also the dominant aerosol component contributing to total aerosol water 37% and 33% respectively, while at XAN sulfate salts were associated with 42% and OA with 32% of the water. Focusing on the inorganic components alone, aerosol water was found to be controlled by nitrate and sulfate. Nitrate had the highest contributions to inorganic aerosol water at IOA (24%), THI (31%), LAP (30%) and PTR (21%). NH$_4$NO$_3$ was the dominant salt at IOA, LAP and PTR; while at THI NaNO$_3$ contributed 25% to the total water associated with inorganics along with NH$_4$NO$_3$ (22%). The situation at FKL was different with chloride and sulfate being the major contributors to aerosol water (40% and 36% respectively), while OA had only a minor contribution (5%) due to its very low concentration at this site. The dominant chloride salt at FKL was NH$_4$Cl contributing 31% to the total inorganic water while Na$_2$SO$_4$ was the major sulfate salt, contributing 17%.

In July and August in the three sites with available observations, sulfate dominated aerosol water (Fig. 7b) with contributions ranging from 70% at IOA to 80% at FKL and THI. (NH$_4$)$_2$SO$_4$ was the dominant salt at all three sites, contributing more than half of the total water content at THI (58%) and 38% and 40% at IOA and FKL, respectively. The second most dominant aerosol component was OA with 19% contribution to the total aerosol water at THI, 27% at IOA and 14% at FKL.

3.4 Sensitivity of pH to NH$_3$ and HNO$_3$

Studies with ISORROPIA-II (Guo et al., 2015, Weber et al., 2016) have shown that neglecting gas-phase NH$_3$ in the thermodynamic equilibrium calculation of pH results in an underestimation of at most one pH unit (Bougiatioti et al., 2016). Due to the lack of in situ measurements of the gas phase NH$_3$ (except PTR) and HNO$_3$ during the campaign periods, a sensitivity test was conducted varying the assumed concentrations of the gases that we used for the aerosol pH estimation. In detail, simulations with half and double the concentrations of NH$_3$ and HNO$_3$ were conducted for all sites during both periods; winter (January) and summer (July and August). The resulted difference in aerosol pH (ΔpH) due to these altered gas phase concentrations are depicted in Fig. 8 and the mean values of ΔpH for each simulation are summarized in Table S8 along with the concentrations of the gases for the base case scenarios (i.e. the concentrations used for the main simulations). For the case of NH$_3$, an average (across all sites and both periods) of 0.25 increase in aerosol pH was observed when double the amount of NH$_3$ introduced to each system and the increase in pH ranged between 0.13 and 0.34 pH units. On the other hand, when half the amount of NH$_3$ was used a smaller change was observed across the sites; the mean decrease in aerosol pH was -

423   0.19 pH units while it ranged from -0.07 to -0.31 units. For the sensitivity simulations varying the amount of

424   HNO₃ the overall change in aerosol pH was much less distinct. The mean decrease in the pH of the aerosol was

425   between 0.01 and 0.15 pH units when the concentration of HNO₃ was doubled (the overall mean decrease was

426   0.06). Using half the concentration of HNO₃ resulted in a mean increase ranging from 0.01 to 0.15 pH units.

427   According to this sensitivity analysis, the uncertainty in the gas phase NH₃ could explain about half of the seasonal

428   difference in aerosol pH that was presented and discussed in section 3.2.4 about the factors affecting the

429   seasonality of pH. The uncertainty in gas phase NH₃ could explain a larger fraction of the seasonal difference in

430   aerosol pH in IOA than in FKL and THI, which is expected since at these two sites aerosol pH seasonality was

431   predominately driven by sulfates. Our results show a factor of 2 uncertainty in NH₃ lead to an average pH

432   difference of 0.25 units that has minor impact on our findings discussed below.

433

434   3.5.1 Sensitivity of PM levels to NH_3 and HNO_3 availability

435   We used the framework developed by Nenes et al. (2020) that relates the levels of aerosol pH with the formation

436   of aerosol nitrate (and ammonium), to investigate the sensitivity of the different aerosol systems studied here to

437   the gas-phase concentrations of NH_3 and HNO_3. The main parameters used in this framework that control the

438   secondary inorganic particulate matter sensitivity are the aerosol pH, liquid water content and temperature. The

439   conceptual idea is that there is a "sensitivity window" of pH levels in which the partitioning of nitrate shifts from

440   nitrate being predominately gaseous to mostly in the aerosol phase. When acidity is below this pH sensitivity

441   window, particulate nitrate is almost non-existent and consequently aerosol levels are insensitive to HNO_3

442   availability. In this case, aerosol reduction policies that only target HNO_3 reduction cannot be effective (Nenes et

443   al., 2020), as there is no nitrate in the aerosol phase. Based on these criteria, this framework defines characteristic

444   levels of aerosol acidity at which the aerosol becomes insensitive to NH_3 (or HNO_3) levels and vice versa.

445   Therefore, four possible regimes of PM sensitivity can be derived; i) neither NH_3 nor HNO_3 are important for PM

446   formation, or PM formation is dominated by ii) HNO_3, iii) both NH_3 and HNO_3, and iv) NH_3 alone.

447   Figure 9 shows the $PM_{2.5}$ sensitivity maps derived using this framework and the daily data at all stations in

448   January 2020 (Fig. 9a) and at FKL, THI and IOA in summer (July and August) (Fig. 9b) (34 days in total; in July

449   and August 2019). Considering the average temperature across the 3 sites (Table S9) the pH sensitivity window

450   for each of the two gases (NH_3 and HNO_3) was calculated as a function of aerosol water (LWC). The data that

451   were used as well as the aerosol pH and water from the combination of the datasets from the 3 sites are given in

452   Table S9.

453   During January, an overall sensitivity of $PM_{2.5}$ to HNO_3 is found as most of the points of the sites reside above

454   the blue line thus an increase in HNO_3 concentration will lead to its partitioning to the aerosol phase as nitrate.

455   On the other hand, most points are also above the red line indicating that $PM_{2.5}$ is relatively insensitive to gas

456   phase NH_3. Depending on the conditions and aerosol acidity levels, each site may have some days that deviate

457   from the HNO_3-only sensitivity region. At FKL out of the 17 days where HNO_3 sensitivity dominated, on 4 days

458    $PM_{2.5}$ was sensitive to both HNO_3 and NH_3 levels due to the slightly more acidic particles present. At THI $PM_{2.5}$

459   was sensitive to HNO_3 on all 27 days that were examined, except for two days in which NH_3 sensitivity regime

460   also occurred and characterized by lower aerosol pH values (2.05 and 2.13 pH units). At IOA as a consequence

461   of the lower aerosol acidity, $PM_{2.5}$ was (as expected) almost exclusively in the HNO_3 sensitive regime where NH_3

mass variations would not affect PM concentration. At IOA, NH_3 availability was found to play a role in aerosol formation in two days when the aerosol water was very high in combination with the aerosol pH being slightly lower. Regions with more acidic particles i.e. XAN and LAP were also in some cases in the HNO_3 and NH_3 sensitive region.

During summer (July and August) $PM_{2.5}$ shifted out of the HNO_3 only sensitive region at all three sites and NH_3 started to play a more important role for the aerosol levels due to the more acidic conditions compared to January. In many days at IOA and some at FKL the sensitivity to HNO_3 and the insensitive regime also seemed to exist when extremely low aerosol water content was present. At THI $PM_{2.5}$ sensitivity showed the least "dispersed" picture compared to the other sites, and $PM_{2.5}$ was exclusively sensitive to NH_3 availability due to the consistently high aerosol acidity conditions. Consequently, for the studied period the inorganic $PM_{2.5}$ levels at THI in winter would be reduced by limitation of HNO_3 formation, which depends on VOC and NO_x conditions, and NH_3 controls in summer. However, sulfate is the major inorganic $PM_{2.5}$ component during the summer so the NH_3 reductions would have a relatively small effect on the total fine PM. The inclusion of the OA in the aerosol pH and water calculations resulted in a small difference in terms of these sensitivity maps. As the aerosol water increased slightly, in a few cases in XAN the PM sensitivity was shifted from insensitive to HNO_3 sensitive, while in a few cases in IOA and FKL, PM also became sensitive to NH_3 (Fig. S6).

3.5.2 Importance of semivolatiles for deposition

Aerosol acidity and water effects on the partitioning of HNO_3 and NH_3 are linked with the total deposition of these species, in both their gas and particulate forms. As HNO_3 and NH_3 are deposited about 10 times faster than their particulate forms (NO_3^-, NH_4^+), the partitioning between gas and particulate phase affects how fast HNO_3/ NO_3^- or NH_3/ NH_4^+ are deposited (Nenes et al., 2021) and therefore the distance to which they are transported within the atmosphere before deposition (Baker et al., 2021). This gas-to-particle partitioning depends on the pH of the aerosol water and on the LWC of the aerosol (Guo et al., 2015). Therefore, "fast" and "slow" deposition regimes for HNO_3 and NH_3 can be defined as a function of aerosol pH and LWC. Figure 10 shows the reactive nitrogen (sum of TNO_3 and TNH_3) deposition regimes at the sites, where data were available both in January (Fig. 10a) and summer (July and August) (Fig. 10b), calculated using the average temperatures of the datasets for each season. Looking at the characterization of the deposition domains for all the studied sites during January, a main difference can be observed in terms of the nitrogen deposition velocity (Fig. 10a). At all sites, NH_3 seems to always experience fast deposition. On the other hand, nitrate's deposition rate varies between fast (as gaseous HNO_3) and slow (as particulate NO_3^-), leading to local removal or long-range transport, respectively. IOA and PTR cases are almost exclusively in the HNO_3 slow – NH_3 fast regime due to the higher aerosol pH levels that enhance HNO_3 partitioning to the particulate phase. The other sites are characterized by high deposition rates for both NH_3 and HNO_3. In summer, the deposition is similarly characterized as fast for both NH_3 and HNO_3 at FKL, THI and IOA due to the higher acidity levels. The higher temperature in summer than in winter also favors the fast removal of both HNO_3 and NH_3, with the exception of one day at IOA characterized by extremely low aerosol pH (below zero), where NH_3 was present in the form of particulate NH_4^+ and thus had a slow deposition velocity. Including the OA in the calculations did not change as much the deposition rates (Fig. S7). In a few cases during January in THI and PTR the deposition rate of HNO_3 shifted from fast to slow due to the addition of OA water.

501

Conclusions

This study was based on PM$_{2.5}$ chemical composition observations in 6 regions of Greece (Finokalia, FKL; Thissio, THI; Patras, PTR; Ioannina, IOA; Xanthi, XAN; and Thessaloniki, LAP) during summer 2019 (in FKL, THI and IOA) and winter 2019-2020 (in all regions) as part of the national research infrastructure PANACEA. The aerosol composition measurements together with the gas phase NH$_3$, HNO$_3$ data were used in the thermodynamic model ISORROPIA-lite to calculate the fine aerosol pH at all the sites and to determine its seasonal variation.

The pH levels of PM$_{2.5}$ across Greece during winter ranged from 1.72 to 5.14. The highest pH values were estimated at IOA (4.08 ± 0.42) and PTR (3.70 ± 0.45) followed by THI (3.30 ± 0.48) and FKL (3.25 ± 0.37), while aerosols at XAN and LAP were the most acidic (2.81 ± 0.53 and 3.01 ± 0.31, respectively). The lowest acidity at IOA was associated with high K$^+$ levels from biomass burning emissions in combination with high Ca^{2+} and NH$_3$ and low temperatures. Similar factors (NH$_3$ and cation levels) affected PTR aerosol pH. The aerosol acidity levels at the urban background site (THI) were similar to those at the coastal background site (FKL). High nonvolatile cation concentrations at FKL, together with elevated humidity levels resulted in a higher mean aerosol pH compared to the rural background site (XAN), which had slightly higher levels of sulfates than FKL.

In summer, PM$_{2.5}$ was generally more acidic than in winter at the three sites studied (THI, IOA and FKL), with mean pH values of 1.35 ± 0.18 (THI), 1.75 ± 0.62 (IOA) and 2.08 ± 0.45 units (FKL). pH in summer was lower than winter by 1 (FKL) to about 2 (THI and IOA) pH units. Sulfates drive the seasonal variation in aerosol pH at THI and FKL. At IOA, on the other hand, temperature together with NH$_3$ and HNO$_3$ availability were the main drivers of the seasonal difference in aerosol acidity, with K$^+$, Ca^{2+}, and sulfates also contributing.

Organics contributed significantly to the total fine aerosol mass at all sites but FKL in January. OA was found to be the main contributor to the total aerosol water at IOA and PTR (60% and 55% contribution, respectively) due to the OA levels in these sites, and the dominant contributor at THI and LAP (33% and 37% contribution respectively). During January nitrate salts contributed more to the total aerosol water at IOA (24%), THI (31%), LAP (30%) and PTR (21%), with NH$_4$NO$_3$ being the dominant salt present at IOA, LAP and PTR and NaNO$_3$ at THI. The aerosol water content at XAN was dominated by sulfate (42%), with OA also contributing to the total aerosol water (32%). Chloride and sulfate contributed more to the aerosol water at FKL (40% and 36% respectively). During summer (July and August), sulfate salts contributed more to LWC at all sites (80% contribution at FKL and THI and 70% at IOA), with (NH$_4$)$_2$SO$_4$ being the dominant species of the inorganic LWC at all three sites. At sites with higher aerosol pH (IOA, THI and PTR in January), the water associated with the organics did not increase aerosol pH in most cases. This behavior associated with aerosol pH above 4 units is the result of increased partitioning of semivolatiles to the aerosol phase and of changes in the activity coefficients. Such conditions are good benchmark for testing the thermodynamic model predictions of pH.

PM$_{2.5}$ mass was sensitive to the availability of total HNO$_3$ at all sites during January 2020. At LAP and XAN, PM mass was also found to be sensitive to NH$_3$. In summer (July and August), PM at all three sites examined showed a strong sensitivity to NH$_3$ due to the low summertime aerosol pH. In some cases, the PM$_{2.5}$ concentrations at FKL and IOA appeared insensitive to both precursor species due to the low water content of the aerosols. PM sensitivity at THI in summer showed a clear dependence on NH$_3$, reflecting the higher summertime aerosol

14

acidity. Our results show that HNO$_3$ levels (could contribute to) regulate PM$_{2.5}$ mass concentration which however was mainly composed by OA and sulfate, hence policies targeted to reduce PM$_{2.5}$ levels in Greece would be more effective by reducing HNO$_3$ levels (i.e. transportation sector) in addition to OA and sulfate.

Finally, our analysis has shown that in Greece NH$_3$ deposition is fast, whereas deposition of HNO$_3$/NO$_3^-$ may occur locally near the sources or remotely by long-range transport, depending on the environmental conditions. How future changes in the meteorological conditions and in air pollutant emissions will affect the aerosol pH and the factors controlling it, as well as atmospheric residence time and deposition of reactive nitrogen in the region, requires further investigation.

Colorblind friendly palettes were used to create the figures according to and described in (Crameri et al., 2020). More information about the abovementioned palettes can be found in https://doi.org/10.5281/zenodo.8409685 (Crameri, 2018).

Code availability. ISORROPIA-lite is openly available at https://www.epfl.ch/labs/lapi/models-and-software/isorropia/

Data availability. Observational data are available upon request by the corresponding site principal investigator.

Competing interests. Some authors are members of the editorial board of journal Atmospheric Chemistry and Physics

Author contributions. AMN collected the data, performed the simulations and wrote the manuscript, MK conceived the study and supervised the work. MK and SP edited the manuscript, AN provided the thermodynamic codes and sensitivity/deposition routines for analysis of the data, and advised on their application/interpretation. MT, EL, KP, KT, IT, CK, FB, AK, KM, GK, NK, NH provided data; all authors provided comments on the manuscript.

References

Baker, A. R., Kanakidou, M., Nenes, A., Myriokefalitakis, S., Croot, P. L., Duce, R. A., Gao, Y., Guieu, C., Ito, A., Jickells, T. D., Mahowald, N. M., Middag, R., Perron, M. M. G., Sarin, M. M., Shelley, R., and Turner, D. R.: Changing atmospheric acidity as a modulator of nutrient deposition and ocean biogeochemistry, Sci. Adv., 7, eabd8800, https://doi.org/10.1126/sciadv.abd8800, 2021.

Bougiatioti, A., Fountoukis, C., Kalivitis, N., Pandis, S. N., Nenes, A., and Mihalopoulos, N.: Cloud condensation nuclei measurements in the marine boundary layer of the Eastern Mediterranean: CCN closure and droplet growth kinetics, Atmos. Chem. Phys., 9, 7053–7066, https://doi.org/10.5194/acp-9-7053-2009, 2009.

Bougiatioti, A., Nikolaou, P., Stavroulas, I., Kouvarakis, G., Weber, R., Nenes, A., Kanakidou, M., and Mihalopoulos, N.: Particle water and pH in the eastern Mediterranean: source variability and implications for nutrient availability, Atmos. Chem. Phys., 16, 4579–4591, https://doi.org/10.5194/acp-16-4579-2016, 2016.

Clegg, S. L., Seinfeld, J. H., and Brimblecombe, P.: Thermodynamic modelling of aqueous aerosols containing electrolytes and dissolved organic compounds, Journal of Aerosol Science, 32, 713–738, https://doi.org/10.1016/S0021-8502(00)00105-1, 2001.

Crameri, F.: Geodynamic diagnostics, scientific visualisation and StagLab 3.0, https://doi.org/10.5194/gmd-2017-328, 20 February 2018.

Crameri, F., Shephard, G. E., and Heron, P. J.: The misuse of colour in science communication, Nat Commun, 11, https://doi.org/10.1038/s41467-020-19160-7, 2020.

Ding, J., Zhao, P., Su, J., Dong, Q., Du, X., and Zhang, Y.: Aerosol pH and its driving factors in Beijing, Atmos. Chem. Phys., 19, 7939–7954, https://doi.org/10.5194/acp-19-7939-2019, 2019.

Fang, T., Guo, H., Zeng, L., Verma, V., Nenes, A., and Weber, R. J.: Highly Acidic Ambient Particles, Soluble Metals, and Oxidative Potential: A Link between Sulfate and Aerosol Toxicity, Environ. Sci. Technol., 51, 2611–2620, https://doi.org/10.1021/acs.est.6b06151, 2017.

Flocas, H., Kelessis, A., Helmis, C., Petrakakis, M., Zoumakis, M., and Pappas, K.: Synoptic and local scale atmospheric circulation associated with air pollution episodes in an urban Mediterranean area, Theor Appl Climatol, 95, 265–277, https://doi.org/10.1007/s00704-008-0005-9, 2009.

Florou, K., Papanastasiou, D. K., Pikridas, M., Kaltsonoudis, C., Louvaris, E., Gkatzelis, G. I., Patoulias, D., Mihalopoulos, N., and Pandis, S. N.: The contribution of wood burning and other pollution sources to wintertime organic aerosol levels in two Greek cities, Atmos. Chem. Phys., 17, 3145–3163, https://doi.org/10.5194/acp-17-3145-2017, 2017.

Fountoukis, C. and Nenes, A.: ISORROPIA II: a computationally efficient thermodynamic equilibrium model for $K^+–Ca^{2+}–Mg^{2+}–NH_4^+ –Na^+–SO_4^{2−}–NO_3^− –Cl^−–H_2O$ aerosols, Atmos. Chem. Phys., 21, 2007.

Guo, H., Xu, L., Bougiatioti, A., Cerully, K. M., Capps, S. L., Hite, J. R., Carlton, A. G., Lee, S.-H., Bergin, M. H., Ng, N. L., Nenes, A., and Weber, R. J.: Fine-particle water and pH in the southeastern United States, Atmos. Chem. Phys., 15, 5211–5228, https://doi.org/10.5194/acp-15-5211-2015, 2015.

Guo, H., Sullivan, A. P., Campuzano-Jost, P., Schroder, J. C., Lopez-Hilfiker, F. D., Dibb, J. E., Jimenez, J. L., Thornton, J. A., Brown, S. S., Nenes, A., and Weber, R. J.: Fine particle pH and the partitioning of nitric acid during winter in the northeastern United States, J. Geophys. Res. Atmos., 121, https://doi.org/10.1002/2016JD025311, 2016.

Guo, H., Liu, J., Froyd, K. D., Roberts, J. M., Veres, P. R., Hayes, P. L., Jimenez, J. L., Nenes, A., and Weber, R. J.: Fine particle pH and gas–particle phase partitioning of inorganic species in Pasadena, California, during the 2010 CalNex campaign, Atmos. Chem. Phys., 17, 5703–5719, https://doi.org/10.5194/acp-17-5703-2017, 2017a.

621   Guo, H., Weber, R. J., and Nenes, A.: High levels of ammonia do not raise fine particle pH sufficiently to yield
622   nitrogen oxide-dominated sulfate production, Sci Rep, 7, 12109, https://doi.org/10.1038/s41598-017-11704-0,
623   2017b.

624   Guo, H., Otjes, R., Schlag, P., Kiendler-Scharr, A., Nenes, A., and Weber, R. J.: Effectiveness of ammonia
625   reduction on control of fine particle nitrate, Atmos. Chem. Phys., 18, 12241–12256, https://doi.org/10.5194/acp-
626   18-12241-2018, 2018.

627   Hildebrandt, L., Kostenidou, E., Lanz, V. A., Prevot, A. S. H., Baltensperger, U., Mihalopoulos, N., Laaksonen,
628   A., Donahue, N. M., and Pandis, S. N.: Sources and atmospheric processing of organic aerosol in the
629   Mediterranean: insights from aerosol mass spectrometer factor analysis, Atmos. Chem. Phys., 11, 12499–12515,
630   https://doi.org/10.5194/acp-11-12499-2011, 2011.

631   Kakavas, S., Patoulias, D., Zakoura, M., Nenes, A., and Pandis, S. N.: Size-resolved aerosol pH over Europe
632   during summer, Atmos. Chem. Phys., 21, 799–811, https://doi.org/10.5194/acp-21-799-2021, 2021.

633   Kakavas, S., Pandis, S. N., and Nenes, A.: ISORROPIA-Lite: A Comprehensive Atmospheric Aerosol
634   Thermodynamics Module for Earth System Models, Tellus B: Chemical and Physical Meteorology, 74, 1–23,
635   https://doi.org/10.16993/tellusb.33, 2022.

636   Kalkavouras, P., Bougiatioti, A., Kalivitis, N., Stavroulas, I., Tombrou, M., Nenes, A., and Mihalopoulos, N.:
637   Regional new particle formation as modulators of cloud condensation nuclei and cloud droplet number in the
638   eastern Mediterranean, Atmos. Chem. Phys., 19, 6185–6203, https://doi.org/10.5194/acp-19-6185-2019, 2019.

639   Kanakidou, M., Myriokefalitakis, S., and Tsigaridis, K.: Aerosols in atmospheric chemistry and biogeochemical
640   cycles of nutrients, Environ. Res. Lett., 13, 063004, https://doi.org/10.1088/1748-9326/aabcdb, 2018.

641   Kaskaoutis, D. G., Grivas, G., Theodosi, C., Tsagkaraki, M., Paraskevopoulou, D., Stavroulas, I., Liakakou, E.,
642   Gkikas, A., Hatzianastassiou, N., Wu, C., Gerasopoulos, E., and Mihalopoulos, N.: Carbonaceous Aerosols in
643   Contrasting Atmospheric Environments in Greek Cities: Evaluation of the EC-tracer Methods for Secondary
644   Organic Carbon Estimation, Atmosphere, 11, 161, https://doi.org/10.3390/atmos11020161, 2020.

645   Kaskaoutis, D. G., Grivas, G., Oikonomou, K., Tavernaraki, P., Papoutsidaki, K., Tsagkaraki, M., Stavroulas, I.,
646   Zarmpas, P., Paraskevopoulou, D., Bougiatioti, A., Liakakou, E., Gavrouzou, M., Dumka, U. C.,
647   Hatzianastassiou, N., Sciare, J., Gerasopoulos, E., and Mihalopoulos, N.: Impacts of severe residential wood
648   burning on atmospheric processing, water-soluble organic aerosol and light absorption, in an inland city of
649   Southeastern Europe, Atmospheric Environment, 280, 119139, https://doi.org/10.1016/j.atmosenv.2022.119139,
650   2022.

651   Kastelis, N. and Kourtidis, K.: Characteristics of the atmospheric electric field and correlation with CO2 at a
652   rural site in southern Balkans, Earth Planet Sp, 68, 3, https://doi.org/10.1186/s40623-016-0379-3, 2016.

653   Kostenidou, E., Florou, K., Kaltsonoudis, C., Tsiflikiotou, M., Vratolis, S., Eleftheriadis, K., and Pandis, S. N.:
654   Sources and chemical characterization of organic aerosol during the summer in the eastern Mediterranean,
655   Atmos. Chem. Phys., 15, 11355–11371, https://doi.org/10.5194/acp-15-11355-2015, 2015.

656   Lemou, A., Rabhi, L., Merabet, H., Ladji, R., Nicolas, J. B., Bonnaire, N., Mustapha, M. A., Dilmi, R., Sciare,
657   J., Mihalopoulos, N., and Yassaa, N.: Chemical characterization of fine particles (PM2.5) at a coastal site in the
658   South Western Mediterranean during the ChArMex experiment, Environ Sci Pollut Res, 27, 20427–20445,
659   https://doi.org/10.1007/s11356-020-08168-7, 2020.

660   Liakakou, E., Fourtziou, L., Paraskevopoulou, D., Speyer, O., Lianou, M., Grivas, G., Myriokefalitakis, S., and
661   Mihalopoulos, N.: High-Resolution Measurements of SO2, HNO3 and HCl at the Urban Environment of
662   Athens, Greece: Levels, Variability and Gas to Particle Partitioning, Atmosphere, 13, 218,
663   https://doi.org/10.3390/atmos13020218, 2022.

664   Liu, M., Song, Y., Zhou, T., Xu, Z., Yan, C., Zheng, M., Wu, Z., Hu, M., Wu, Y., and Zhu, T.: Fine particle pH
665   during severe haze episodes in northern China: Fine Particle pH During Haze Episodes, Geophys. Res. Lett., 44,
666   5213–5221, https://doi.org/10.1002/2017GL073210, 2017.

Masiol, M., Squizzato, S., Formenton, G., Khan, M. B., Hopke, P. K., Nenes, A., Pandis, S. N., Tositti, L., Benetello, F., Visin, F., and Pavoni, B.: Hybrid multiple-site mass closure and source apportionment of PM2.5 and aerosol acidity at major cities in the Po Valley, Science of The Total Environment, 704, 135287, https://doi.org/10.1016/j.scitotenv.2019.135287, 2020.

Mihalopoulos, N., Stephanou, E., Kanakidou, M., Pilitsidis, S., and Bousquet, P.: Tropospheric aerosol ionic composition in the Eastern Mediterranean region, Tellus B, 49, 314–326, https://doi.org/10.1034/j.1600-0889.49.issue3.7.x, 1997.

Nenes, A., Pandis, S. N., Weber, R. J., and Russell, A.: Aerosol pH and liquid water content determine when particulate matter is sensitive to ammonia and nitrate availability, Atmos. Chem. Phys., 20, 3249–3258, https://doi.org/10.5194/acp-20-3249-2020, 2020.

Nenes, A., Pandis, S. N., Kanakidou, M., Russell, A. G., Song, S., Vasilakos, P., and Weber, R. J.: Aerosol acidity and liquid water content regulate the dry deposition of inorganic reactive nitrogen, Atmos. Chem. Phys., 21, 6023–6033, https://doi.org/10.5194/acp-21-6023-2021, 2021.

Paglione, M., Decesari, S., Rinaldi, M., Tarozzi, L., Manarini, F., Gilardoni, S., Facchini, M. C., Fuzzi, S., Bacco, D., Trentini, A., Pandis, S. N., and Nenes, A.: Historical Changes in Seasonal Aerosol Acidity in the Po Valley (Italy) as Inferred from Fog Water and Aerosol Measurements, Environ. Sci. Technol., 55, 7307–7315, https://doi.org/10.1021/acs.est.1c00651, 2021.

Pikridas, M., Bougiatioti, A., Hildebrandt, L., Engelhart, G. J., Kostenidou, E., Mohr, C., Prévôt, A. S. H., Kouvarakis, G., Zarmpas, P., Burkhart, J. F., Lee, B.-H., Psichoudaki, M., Mihalopoulos, N., Pilinis, C., Stohl, A., Baltensperger, U., Kulmala, M., and Pandis, S. N.: The Finokalia Aerosol Measurement Experiment – 2008 (FAME-08): an overview, Atmos. Chem. Phys., 10, 6793–6806, https://doi.org/10.5194/acp-10-6793-2010, 2010.

Pikridas, M., Tasoglou, A., Florou, K., and Pandis, S. N.: Characterization of the origin of fine particulate matter in a medium size urban area in the Mediterranean, Atmospheric Environment, 80, 264–274, https://doi.org/10.1016/j.atmosenv.2013.07.070, 2013.

Powley, H. R., Cappellen, P. V., and Krom, M. D.: Nutrient Cycling in the Mediterranean Sea: The Key to Understanding How the Unique Marine Ecosystem Functions and Responds to Anthropogenic Pressures, in: Mediterranean Identities - Environment, Society, Culture, edited by: Fuerst-Bjelis, B., InTech, https://doi.org/10.5772/intechopen.70878, 2017.

Psichoudaki, M., Nenes, A., Florou, K., Kaltsonoudis, C., and Pandis, S. N.: Hygroscopic properties of atmospheric particles emitted during wintertime biomass burning episodes in Athens, Atmospheric Environment, 178, 66–72, https://doi.org/10.1016/j.atmosenv.2018.01.004, 2018.

Putaud, J.-P., Raes, F., Van Dingenen, R., Brüggemann, E., Facchini, M.-C., Decesari, S., Fuzzi, S., Gehrig, R., Hüglin, C., Laj, P., Lorbeer, G., Maenhaut, W., Mihalopoulos, N., Müller, K., Querol, X., Rodriguez, S., Schneider, J., Spindler, G., Brink, H. T., Tørseth, K., and Wiedensohler, A.: A European aerosol phenomenology—2: chemical characteristics of particulate matter at kerbside, urban, rural and background sites in Europe, Atmospheric Environment, 38, 2579–2595, https://doi.org/10.1016/j.atmosenv.2004.01.041, 2004.

Pye, H. O. T., Nenes, A., Alexander, B., Ault, A. P., Barth, M. C., Clegg, S. L., Collett, J. L., Fahey, K. M., Hennigan, C. J., Herrmann, H., Kanakidou, M., Kelly, J. T., Ku, I. T., Faye McNeill, V., Riemer, N., Schaefer, T., Shi, G., Tilgner, A., Walker, J. T., Wang, T., Weber, R., Xing, J., Zaveri, R. A., and Zuend, A.: The acidity of atmospheric particles and clouds, Atmospheric Chemistry and Physics, 20, 4809–4888, https://doi.org/10.5194/acp-20-4809-2020, 2020.

Sciare, J., Oikonomou, K., Favez, O., Liakakou, E., Markaki, Z., Cachier, H., and Mihalopoulos, N.: Long-term measurements of carbonaceous aerosols in the Eastern Mediterranean: evidence of long-range transport of biomass burning, Atmos. Chem. Phys., 2008.

Seinfeld, J. H. and Pandis, S. N.: Atmospheric chemistry and physics: from air pollution to climate change, 2nd ed., J. Wiley, Hoboken, N.J, 1203 pp., 2006.

Shephard, M. W. and Cady-Pereira, K. E.: Cross-track Infrared Sounder (CrIS) satellite observations of tropospheric ammonia, Atmos. Meas. Tech., 8, 1323–1336, https://doi.org/10.5194/amt-8-1323-2015, 2015.

Shephard, M. W., Dammers, E., Cady-Pereira, K. E., Kharol, S. K., Thompson, J., Gainariu-Matz, Y., Zhang, J., McLinden, C. A., Kovachik, A., Moran, M., Bittman, S., Sioris, C. E., Griffin, D., Alvarado, M. J., Lonsdale, C., Savic-Jovcic, V., and Zheng, Q.: Ammonia measurements from space with the Cross-track Infrared Sounder: characteristics and applications, Atmos. Chem. Phys., 20, 2277–2302, https://doi.org/10.5194/acp-20-2277-2020, 2020.

Shi, G., Xu, J., Peng, X., Xiao, Z., Chen, K., Tian, Y., Guan, X., Feng, Y., Yu, H., Nenes, A., and Russell, A. G.: pH of Aerosols in a Polluted Atmosphere: Source Contributions to Highly Acidic Aerosol, Environ. Sci. Technol., 51, 4289–4296, https://doi.org/10.1021/acs.est.6b05736, 2017.

Squizzato, S., Masiol, M., Brunelli, A., Pistollato, S., Tarabotti, E., Rampazzo, G., and Pavoni, B.: Factors determining the formation of secondary inorganic aerosol: a case study in the Po Valley (Italy), Atmos. Chem. Phys., 13, 1927–1939, https://doi.org/10.5194/acp-13-1927-2013, 2013.

Stavroulas, I., Bougiatioti, A., Grivas, G., Paraskevopoulou, D., Tsagkaraki, M., Zarmpas, P., Liakakou, E., Gerasopoulos, E., and Mihalopoulos, N.: Sources and processes that control the submicron organic aerosol composition in an urban Mediterranean environment (Athens): a high temporal-resolution chemical composition measurement study, Atmos. Chem. Phys., 19, 901–919, https://doi.org/10.5194/acp-19-901-2019, 2019.

Tao, Y. and Murphy, J. G.: The sensitivity of PM$_{2.5}$ acidity to meteorological parameters and chemical composition changes: 10-year records from six Canadian monitoring sites, Atmos. Chem. Phys., 19, 9309–9320, https://doi.org/10.5194/acp-19-9309-2019, 2019.

Theodosi, C., Markaki, Z., and Mihalopoulos, N.: Iron speciation, solubility and temporal variability in wet and dry deposition in the Eastern Mediterranean, Marine Chemistry, 120, 100–107, https://doi.org/10.1016/j.marchem.2008.05.004, 2008.

Tsiflikiotou, M. A., Kostenidou, E., Papanastasiou, D. K., Patoulias, D., Zarmpas, P., Paraskevopoulou, D., Diapouli, E., Kaltsonoudis, C., Florou, K., Bougiatioti, A., Stavroulas, I., Theodosi, C., Kouvarakis, G., Vasilatou, V., Siakavaras, D., Biskos, G., Pilinis, C., Eleftheriadis, K., Gerasopoulos, E., Mihalopoulos, N., and Pandis, S. N.: Summertime particulate matter and its composition in Greece, Atmospheric Environment, 213, 597–607, https://doi.org/10.1016/j.atmosenv.2019.06.013, 2019.

Vierke, L., Ahrens, L., Shoeib, M., Palm, W.-U., Webster, E. M., Ellis, D. A., Ebinghaus, R., and Harner, T.: In situ air–water and particle–water partitioning of perfluorocarboxylic acids, perfluorosulfonic acids and perfluorooctyl sulfonamide at a wastewater treatment plant, Chemosphere, 92, 941–948, https://doi.org/10.1016/j.chemosphere.2013.02.067, 2013.

Warner, J. X., Wei, Z., Strow, L. L., Dickerson, R. R., and Nowak, J. B.: The global tropospheric ammonia distribution as seen in the 13-year AIRS measurement record, Atmos. Chem. Phys., 16, 5467–5479, https://doi.org/10.5194/acp-16-5467-2016, 2016.

Weber, R. J., Guo, H., Russell, A. G., and Nenes, A.: High aerosol acidity despite declining atmospheric sulfate concentrations over the past 15 years, Nature Geosci, 9, 282–285, https://doi.org/10.1038/ngeo2665, 2016.

Wexler, A. S.: Atmospheric aerosol models for systems including the ions H^+, NH_4^+, Na^+, SO_4^{2-}, NO_3^-, Cl^-, Br^-, and H_2O, J. Geophys. Res., 107, 4207, https://doi.org/10.1029/2001JD000451, 2002.

Zaveri, R. A., Easter, R. C., Fast, J. D., and Peters, L. K.: Model for Simulating Aerosol Interactions and Chemistry (MOSAIC), J. Geophys. Res., 113, D13204, https://doi.org/10.1029/2007JD008782, 2008.

Zhang, A., Wang, Y., Zhang, Y., Weber, R. J., Song, Y., Ke, Z., and Zou, Y.: Modeling the global radiative effect of brown carbon: a potentially larger heating source in the tropical free troposphere than black carbon, Atmos. Chem. Phys., 20, 1901–1920, https://doi.org/10.5194/acp-20-1901-2020, 2020.

759
760
761
762
763
764
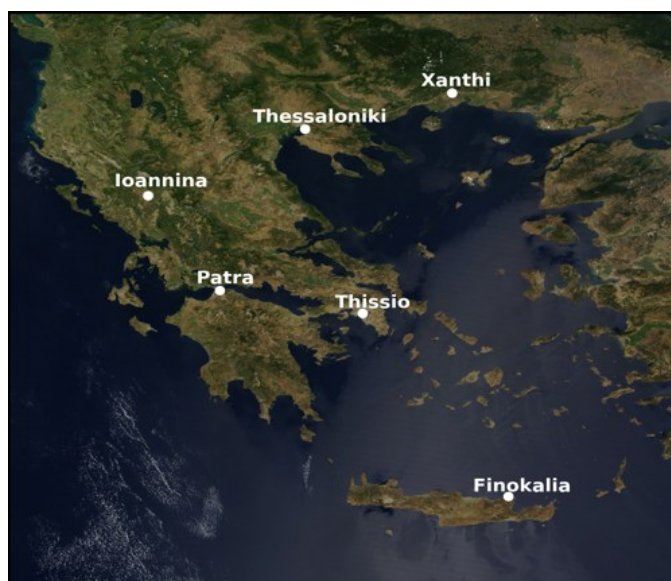765
766
767
768
769
770
771
772
773
774

Figure 1: Map of the region of Greece and the sampling sites. From south to north, Finokalia (FKL), Thissio (THI), Patras (PTR), Ioannina (IOA), Thessaloniki (LAP) and Xanthi (XAN). Original satellite image of Greece obtained from (https://upload.wikimedia.org/wikipedia/commons/9/92/Satellite_image_of_Greece.jpg)

775
776
777

778
779
780
781

Table 1: Descriptive statistics (mean ± stdev) for the chemical composition of $PM_{2.5}$ during the winter and summer PANACEA campaigns. *OA* is the *organic aerosol* derived from OC measurements and a ratio of O*A*/OC of 1.8. Meteorological conditions are also provided. (*) The aerosol pH and LWC calculated with ISORROPIA-lite are also provided (n= number of days).

| *Observations*	FKL		THI		PTR	IOA		LAP	XAN
µg/m³	winter	summer	winter	summer	winter	winter	summer	winter	winter
OA	0.69 ± 0.49	2.91 ± 1.10	4.77 ± 4.53	7.51 ± 5.27	17.35 ± 7.61	50.36 ± 34.46	5.06 ± 1.77	12.45 ± 7.97	6.78 ± 3.33
Na^+	0.39 ± 0.25	0.46 ± 0.33	0.24 ± 0.11	0.17 ± 0.13	0.32 ± 0.30	0.19 ± 0.11	0.12 ± 0.06	0.46 ± 0.49	0.14 ± 0.38
NH_4^+	0.20 ± 0.25	0.99 ± 0.37	0.40 ± 0.25	1.46 ± 0.50	0.67 ± 0.43	1.12 ± 0.81	0.79 ± 0.33	1.04 ± 0.76	0.75 ± 0.58
K^+	0.18 ± 0.24	0.25 ± 0.13	0.29 ± 0.24	0.12 ± 0.05	0.75 ± 0.43	1.45 ± 1.00	0.27 ± 0.18	0.37 ± 0.17	0.30 ± 0.16
Ca^{2+}	0.27 ± 0.40	0.18 ± 0.14	0.23 ± 0.24	0.23 ± 0.20	0.34 ± 0.44	0.96 ± 0.78	0.55 ± 0.25	0.33 ± 0.11	0.17 ± 0.06
Mg^{2+}	0.10 ± 0.12	0.06 ± 0.03	0.02 ± 0.02	0.06 ± 0.01	0.03 ± 0.04	0.03 ± 0.02	0.04 ± 0.01	0.04 ± 0.01	0.04 ± 0.02
SO_4^{2-}	1.30 ± 0.59	3.71 ± 1.18	0.77 ± 0.43	4.42 ± 1.59	1.78 ± 0.90	2.77 ± 1.42	3.27 ± 1.02	2.05 ± 1.00	1.90 ± 1.36
NO_3^-	0.30 ± 0.30	0.14 ± 0.11	0.66 ± 0.50	0.16 ± 0.09	1.39 ± 0.78	3.66 ± 2.73	0.17 ± 0.07	2.01 ± 1.71	0.70 ± 0.58
Cl^-	0.37 ± 0.47	0.31 ± 0.30	0.40 ± 0.19	0.40 ± 0.12	0.25 ± 0.27	0.61 ± 0.38	0.26 ± 0.07	0.33 ± 0.14	0.40 ± 0.18
T (ºC)	11.83 ± 2.74	24.84 ± 1.66	10.64 ± 3.22	28.97 ± 1.90	11.14 ± 2.36	7.43 ± 2.52	26.86 ± 2.60	9.94 ± 2.65	8.62 ± 2.90
RH (%)	72.03 ± 9.68	65.82 ± 9.66	65.85 ± 11.65	46.04 ± 6.69	64.66 ± 11.97	68. 06 ± 20.25	51.59 ± 9.73	57.62 ± 13.17	62.43 ± 16.88
Month (number of samples)	January (n=16)	July & August (n=34)	January (n=27)	July & August (n=34)	January (n=16)	January (n=27)	July & August (n=34)	January (n=4)	January (n=26)
pH*	3.25 ± 0.37	2.08 ± 0.37	3.30 ± 0.48	1.38 ± 0.18	3.70 ± 0.45	4.08 ± 0.42	1.82 ± 0.65	3.01 ± 0.31	2.81 ± 0.53
LWC (µg/m³)*	6.85 ± 3.65	5.85 ± 3.05	3.06 ± 2.96	3.34 ± 1.62	7.00 ± 5.36	56.61 ± 127.59	1.97 ± 0.79	29.68 ± 32.67	4.57 ± 4.29

782
783
784

785
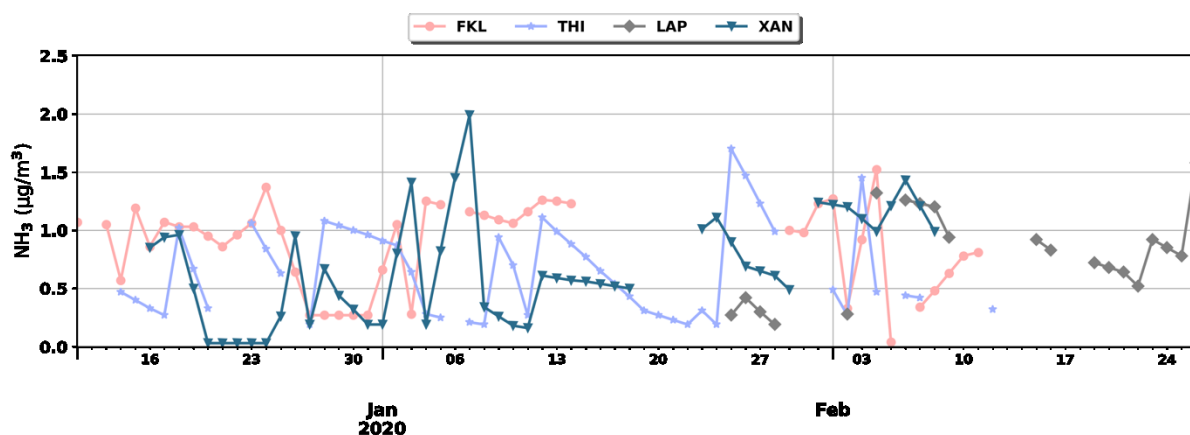
786 **Figure 2: Daily surface NH₃ concentrations during the winter of 2019-2020 as derived from the Cross-track Infrared**
787 **Sounder (CrIS) instrument for FKL, THI, LAP and XAN.**
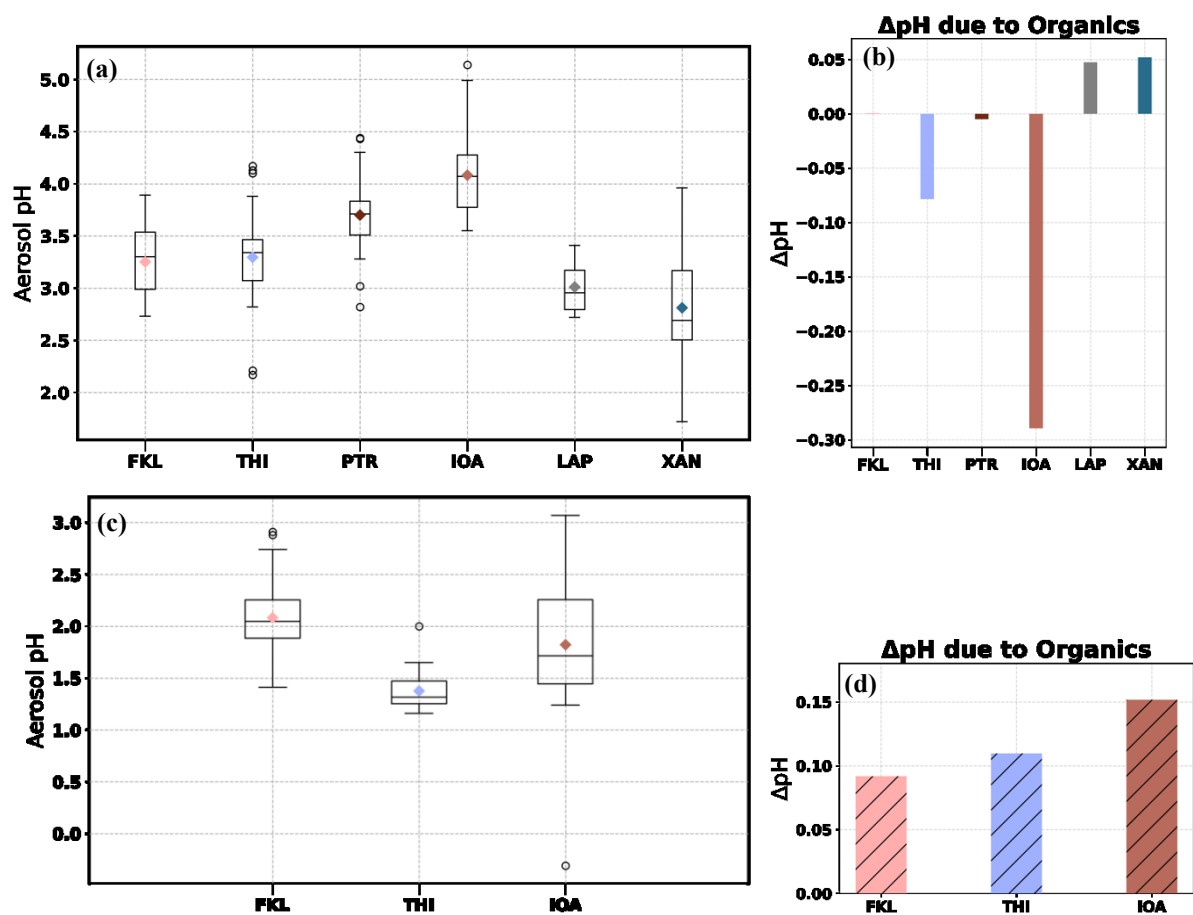
788

789

791

792 **Figure 3: a) and c) total aerosol pH (meaning the aerosol pH associated with inorganics and organics) derived using**
793 **ISORROPIA-lite in January 2020 and summer 2019 (July and August) respectively, b) and d) ΔpH = total aerosol pH**
794 **– inorganic aerosol pH both derived from ISORROPIA-lite in January 2020 and summer 2019 respectively. The**
795 **inorganic aerosol pH was derived by setting the organic concentration and hygroscopicity as zero.**

796
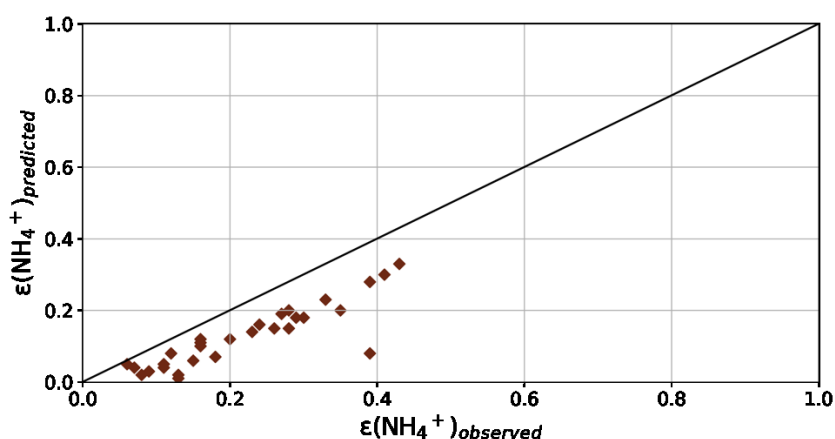
797 **Figure 4: Evaluation of the ISORROPIA-lite results for the case of PTR in winter. Comparison of the partitioning**
798 **coefficient of NH$_4^+$ calculated from measurements with that from the predicted concentrations derived from the model**
799 **(R^2 = 0.78 and y = 0.70x - 0.03). The partitioning coefficient is defined as ε(NH$_4^+$) = NH$_4^+$/(NH$_4^+$ + NH$_3$).** *The black line*
800 *shows the 1:1 ratio.*

801

802

803

804

805 (a)

806 (b)
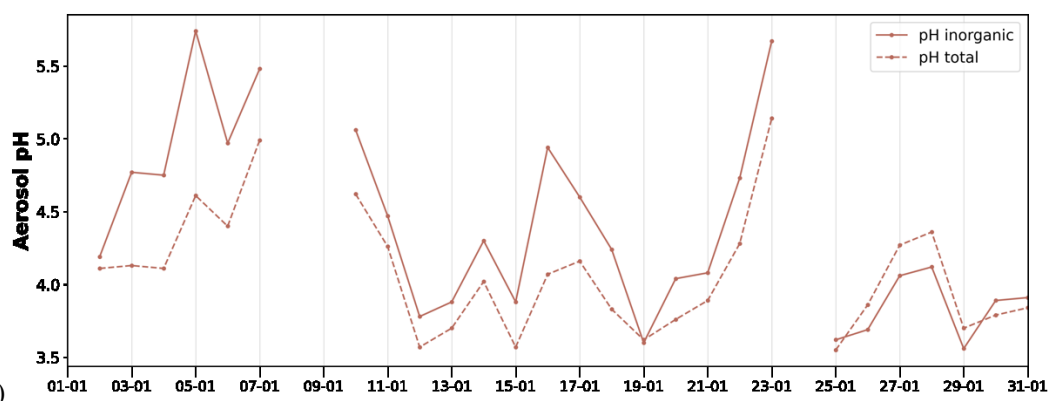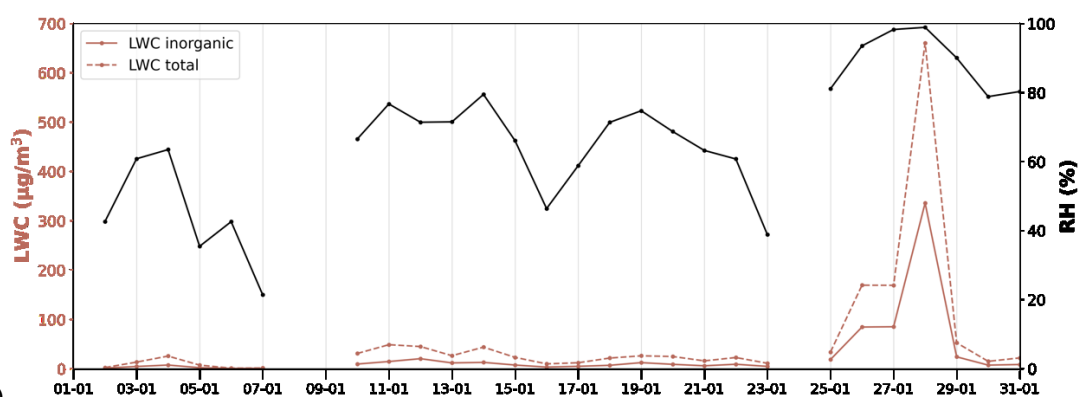
807 **Figure 5: (a) Aerosol liquid water content at IOA in January 2020 as derived from ISORROPIA-lite associated with**
808 **inorganics (inorganic,** *red line***), associated with both inorganics and organics (total,** *red- dashed line***) and relative**
809 **humidity levels (secondary y axis,** *black line***). (b) Inorganic** *(red line)* **and total (***red dashed line,* **associated with**
810 **inorganics and organics) aerosol pH at IOA in January 2020.**
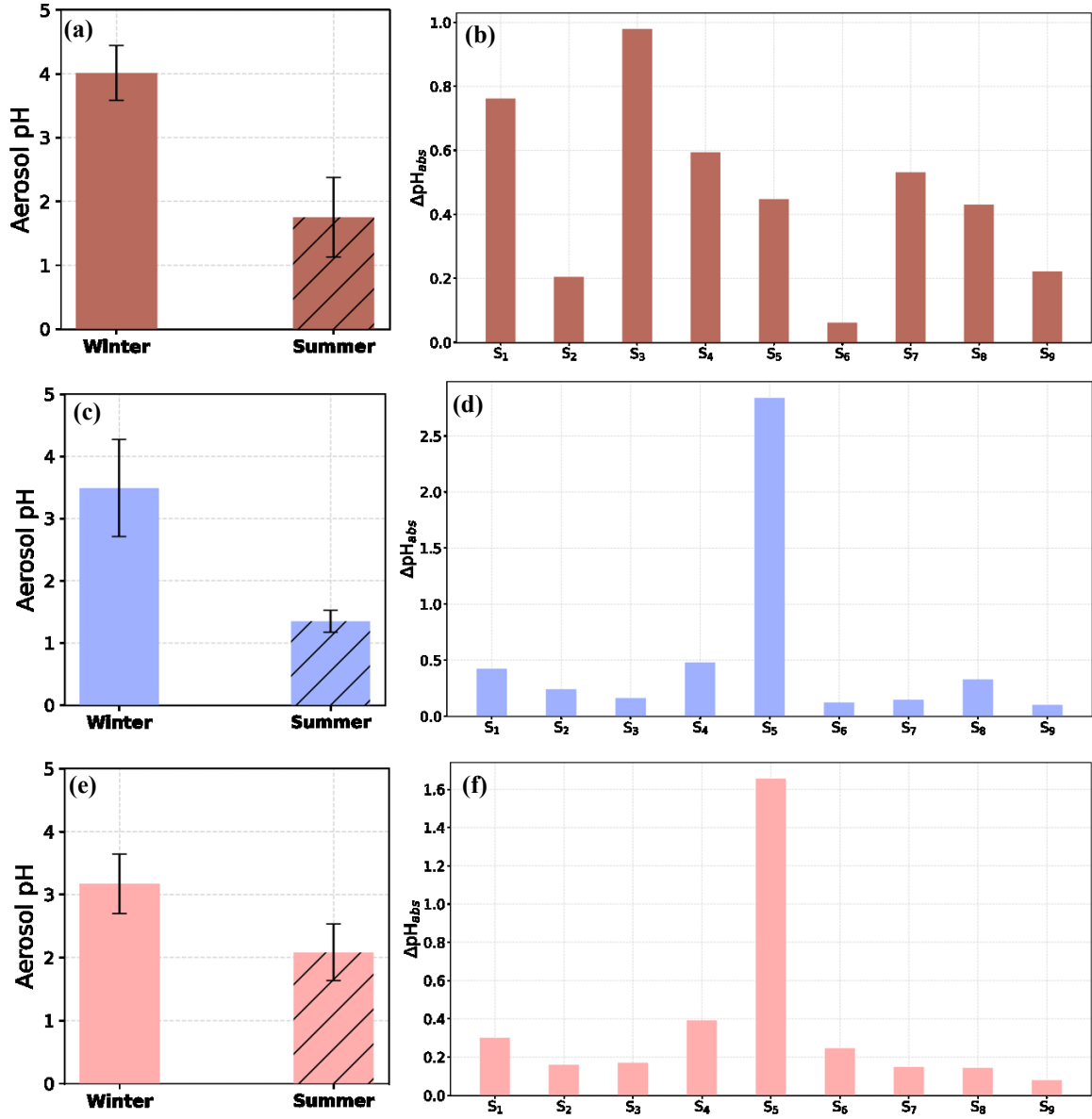
811

812

813

Figure 6: Mean fine aerosol pH in winter and in summer at (a) IOA (c) THI, (e) FKL and the respective sensitivity results for winter conducted for each site (Tables S5 - S7). $\Delta pH_{abs} = |pH_{winter} - pH_{winter(summerX)}|$, where summerX is the mean summer temperature (first simulation, S_1), relative humidity (S_2), TNO_3 (S_3), TNH_3 (S_4), SO_4^{2-} (S_5), Na^+ (S_6), K^+ (S_7), Ca^{2+} (S_8) and OA concentration (S_9) in IOA (b), THI (d) and FKL (f).

825 (a)
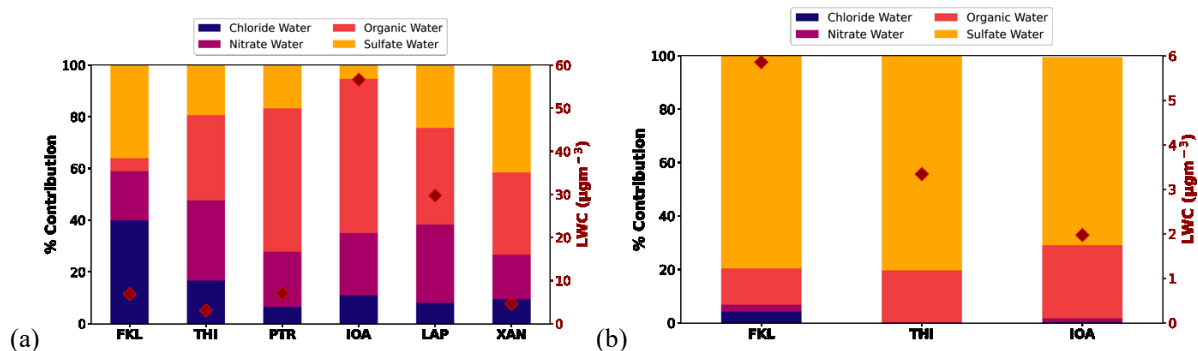
826 **Figure 7: Averaged aerosol liquid water content (LWC) for all sites in winter, January 2020 (a) and summer, July and**
827 **August 2019 (b) expressed as the contribution of each chemical aerosol salt group considering both the inorganics and**
828 **organics at the observational sites shown in Fig. 1 (left axis). Aerosol water mean concentrations are shown with**
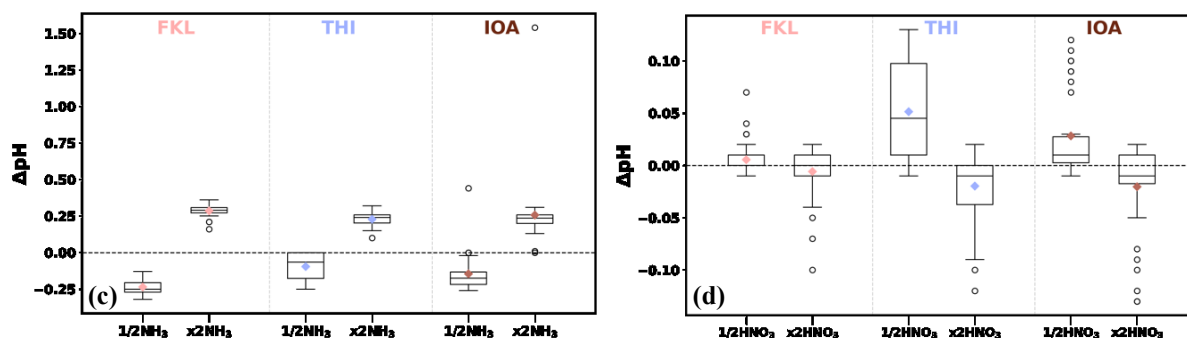829 **rhombus in each plot (right axis).**

830

831

832

833
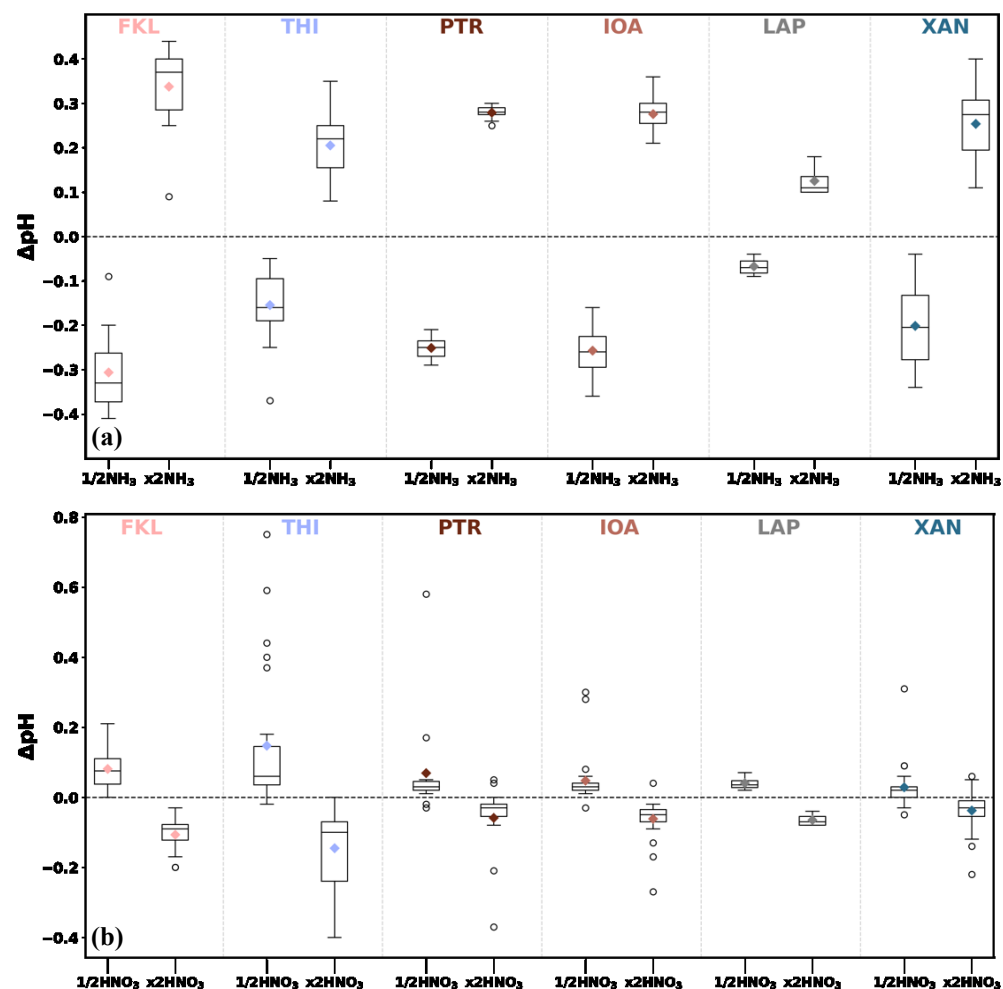
Figure 8: Sensitivity of pH estimation to gas phase NH₃ and HNO₃ concentrations. (a) and (b) are the wintertime (January) simulations for NH₃ and HNO₃ tests respectively and (c) and (d) for the summertime ones (July and August). Each graph shows the difference in pH when using half or double the concentration of the respective gas compared to the original pH at each site. ($\Delta pH = pH_{1/2gas} - pH_{original}$ and $\Delta pH = pH_{x2gas} - pH_{original}$ respectively).
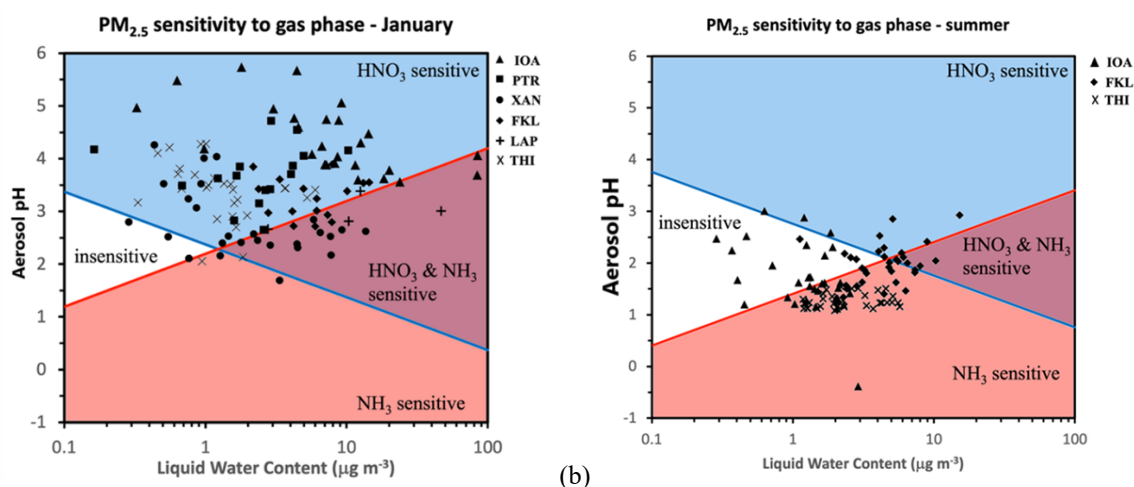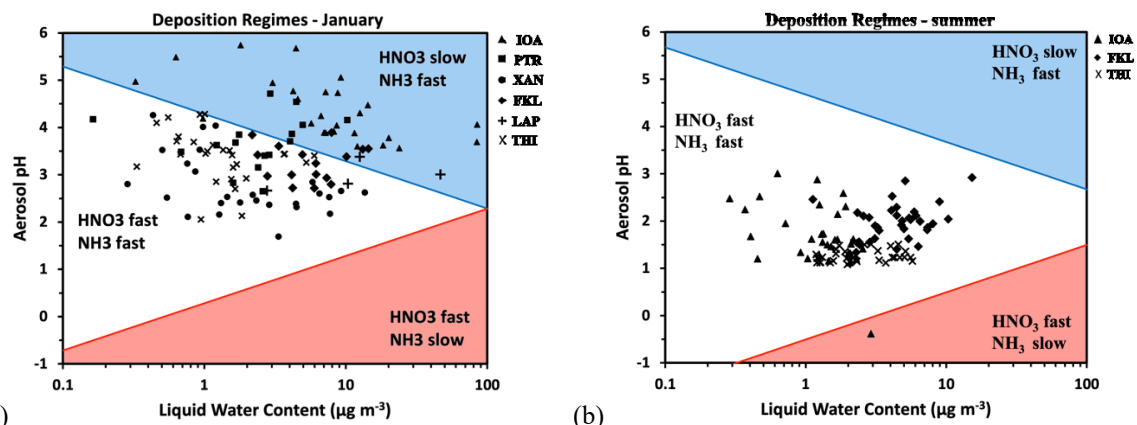

Figure 9: Chemical domains of sensitivity of PM$_{2.5}$ *mass* to NH₃ and NO$_x$ emissions for the studied period (a) in winter (January) and (b) in summer (July and August). The average temperature used here is the mean measured one for the studied period at all sites in each season. Daily averaged values in each season of aerosol pH and liquid water content were used. *The red line shows the characteristic aerosol pH as a function of liquid water content below which the PM$_{2.5}$ mass is sensitive to NH₃ levels and the blue line the characteristic aerosol pH as a function of liquid water content above which the PM$_{2.5}$ mass is sensitive to HNO₃ levels.*

25

863   (a)   (b)

864 **Figure 10: Domains of reactive nitrogen deposition for the studied period (a) in winter (January) and (b) in summer**
865 **(July and August). The average temperature used here is the mean measured one at all sites, for each season. Daily**
866 **averaged values in each season for aerosol pH and liquid water content were used.** *The red line shows the characteristic*
867 *aerosol pH, as a function of liquid water content, below which NH₃ deposition is slow and the blue line the characteristic*
868 *aerosol pH, as a function of liquid water content, above which HNO₃ deposition is slow.*

869

870